ELSEVIER

Research Paper

Oort cloud perturbations as a source of hyperbolic Earth impactors

Eloy Peña-Asensio [a,b,*], Jaakko Visuri [c], Josep M. Trigo-Rodríguez [b,d], Hector Socas-Navarro [e,f], Maria Gritsevich [g,h], Markku Siljama [c], Albert Rimola [a]

[a] *Departament de Química, Universitat Autònoma de Barcelona, Carrer dels Til·lers, Bellaterra, 08193, Catalonia, Spain*
[b] *Institut de Ciències de l'Espai (ICE, CSIC), Campus UAB, C/ de Can Magrans S/N, Cerdanyola del Vallès, 08193, Catalonia, Spain*
[c] *Finnish Fireball Network, Ursa Astronomical Association, Kopernikuksentie 1, Helsinki, 00130, Finland*
[d] *Institut d'Estudis Espacials de Catalunya (IEEC), Carrer del Gran Capità, 2, Barcelona, 08034, Catalonia, Spain*
[e] *Instituto de Astrofísica de Canarias, Avda Vía Láctea S/N, La Laguna, 38205, Tenerife, Spain*
[f] *Departamento de Astrofísica, Universidad de La Laguna, Avda Vía Láctea S/N, La Laguna, 38205, Tenerife, Spain*
[g] *Finnish Geospatial Research Institute, Vuorimiehentie 5, Espoo, 02150, Finland*
[h] *Faculty of Science, University of Helsinki, Gustaf Hällströmin katu 2a, Helsinki, 00014, Finland*

ARTICLE INFO

ABSTRACT

The observation of interstellar objects 1I/'Oumuamua and 2I/Borisov suggests the existence of a larger population of smaller projectiles that impact our planet with unbound orbits. We analyze an asteroidal grazing meteor (FH1) recorded by the Finnish Fireball Network on October 23, 2022. FH1 displayed a likely hyperbolic orbit lying on the ecliptic plane with an estimated velocity excess of ~0.7 km s^{-1} at impact. FH1 may either be an interstellar object, indicating a high-strength bias in this population, or an Oort cloud object, which would reinforce migration-based solar system models. Furthermore, under the calculated uncertainties, FH1 could potentially be associated with the passage of Scholz's binary star system. Statistical evaluation of uncertainties in the CNEOS database and study of its hyperbolic fireballs reveals an anisotropic geocentric radiant distribution and low orbital inclinations, challenging the assumption of a randomly incoming interstellar population. Orbital integrations suggest that the event on March 9, 2017 (IM2) from CNEOS may have experienced gravitational perturbation during the Scholz fly-by, contingent upon velocity overestimation within the expected range. These findings suggest that apparent interstellar meteors may, in fact, be the result of accelerated meteoroid impacts caused by close encounters with massive objects within or passing through our solar system.

1. Introduction

In 2017, the Pan-STARRS1 telescope observed for the first time the reflected sunlight from a metric (~100 m) interstellar interloper, 1I/'Oumuamua (Meech et al., 2017). Two years later, the second discovery of a large object (0.4–1 km) not gravitationally bound to the Sun, comet 2I/Borisov, was announced (Guzik et al., 2020). The discoverer of 2I/Borisov himself estimated that a spherical volume of 50 au radius may have 50 bodies of more than 50 meters in diameter (Borisov and Shustov, 2021). The Pan-STARRS survey's detection of 1I/'Oumuamua allows the calculation of a number density of 0.1 au^{-3}, corresponding to 10^4 similar objects within Neptune's orbit and an influx of 3 objects per day (Jewitt et al., 2017). By the expected power laws of object size distribution, a much more abundant population of smaller interstellar objects is expected to cross our solar system, which may eventually collide with the Earth. A review of interstellar objects and interlopers can be found in Jewitt and Seligman (2023) and Seligman and Moro-Martín (2023).

When an object impacts the atmosphere at hypervelocity, friction with air particles progressively ablates the outer layers, radiating large amounts of energy (Ceplecha et al., 1998; Silber et al., 2018; Trigo-Rodríguez, 2019). This luminous phase is known as a meteor or fireball, and its detection with ground-based or satellite instruments allows both the physicochemical analysis and the determination of the heliocentric orbit (Jenniskens et al., 2009; Trigo-Rodríguez et al., 2006; Dmitriev et al., 2015; Brown et al., 2016; Devillepoix et al., 2019; Borovička et al., 2020; Colas et al., 2020; Peña-Asensio et al., 2021a). Recently, the first detections of interstellar meteors were claimed from the flashes spotted by the U.S. Department of Defense (DoD) satellite sensors and published on the NASA-JPL Center for NEOs Studies (CNEOS)

---

website (Tagliaferri et al., 1994): the so-called IM1 occurred in 2014-01-08 (Siraj and Loeb, 2022a) and IM2 in 2017-03-09 (Siraj and Loeb, 2022b), the latter being first identified as an interstellar candidate by Peña-Asensio et al. (2022).

In the early 20th century, the field of meteor science was predominantly focused on determining whether most meteors originated from interstellar or interplanetary sources (Hughes, 1982). However, it was not until the 1950s that the optical observations of fireballs generated by meteoroids exhibiting hyperbolic were reported (Öpik, 1950; Almond et al., 1951, 1952), in addition to subsequent meteor radar echoes detection of interstellar micrometeoroid impacts (Weryk and Brown, 2004; Froncisz et al., 2020) and interstellar dust incoming flux measurements (Meisel et al., 2002a,b). Multiple automated meteor networks have detected numerous hyperbolic Earth impactors, most of which are pointed out as the result of the instrument and method limitations (Štohl, 1970; Hajduková, 2008; Musci et al., 2012). Hajduková et al. (2020) reported that, of the total number of recorded events, 12.5% for CAMS, 11.9% for SonotaCO, and 5.4% for EDMOND were apparently hyperbolics. These events are clearly associated with low-quality detection and low angular elongation, so these large datasets cannot be used to discern hyperbolic impactors properly, and truly interstellar projectiles could remain hidden within the error bars. The identification of meteors with extra-solar provenance is a significant challenge and statements about the interstellar origin of IM1 and IM2 cannot be conclusive if the uncertainties of the data are not provided (Vaubaillon, 2022). Recent studies have even suggested that IM1 could be consistent with a common chondritic impactor assuming a lower atmospheric entry velocity (Brown and Borovička, 2023).

Peña-Asensio et al. (2022) and Brown and Borovička (2023) identified hyperbolic fireballs recorded by the United States Government (USG) satellite sensors, representing ~1% of total meter-sized impactors, events that are potentially meteorite-droppers. In contrast, there is no evidence of any recovered meteorite with a different composition from that of our solar nebula.[1] This fact opens several hypotheses: (1) CNEOS hyperbolic fireballs are spurious data; (2) There is a viable way for nearby stellar systems to be isotopically homogeneous so extra-solar objects do not have distinctive non-chondritic elemental and isotopic compositions. The interstellar material exchange would be enough to smooth out any differences in the initial inventory of elements; (3) Incoming interstellar objects are biased towards low-strength properties and do not survive either the interstellar medium or the ablation process during the atmospheric entry; (4) There is an efficient mechanism by which objects that belong to our solar nebula acquire hyperbolic orbits.

In this work, we present evidence supporting the latter hypothesis, assuming that the former remains unverified, a matter still awaiting clarification. We show that apparent interstellar meteors may actually be the result of accelerated projectile impacts due to gravitational perturbations induced by massive objects (stars, free-floating brown dwarfs, rogue planets, sub-stellar or sub-Jovian mass perturbers, primordial black holes...) shaping or visiting the outer part of our solar system. In particular, we analyze a likely hyperbolic asteroid-like grazing meteor recorded in Finland in 2022 exhibiting no deceleration, which could be associated with Scholz passage. Additionally, we discuss the IM2 hyperbolic fireballs of the CNEOS database, which may belong either to the Oort cloud or to a hypothetical Oort-like Scholz's cloud if its velocity is overestimated by 22%. All events exhibit non-cometary compositions and probably are not of extra-solar provenance, which has profound implications for solar system formation models. In case they were truly interstellar in origin, the bias towards a high-strength composition of the incoming interstellar population would be reinforced.

---

[1] On the other hand, whenever a meteorite is recovered it is attributed to our solar system by default.

2. Methodology

For the meteor science performed in this work, we use our verified Python pipeline *3D-FireTOC* (Peña-Asensio et al., 2021a,b) which: performs the meteor positional reduction from the stellar astrometry accounting for asymmetric radial lens distortions (Borovicka et al., 1995) and atmospheric refraction by a revised Bennett's model (Wilson, 2018), employs the plane intersection method to reconstruct the atmospheric trajectory (Ceplecha, 1987), and computes the heliocentric orbit using the N-body orbital dynamics integrator *REBOUND* and *REBOUNDx* packages considering the gravitational harmonics (J2, J4) of the Earth and the Moon (Rein and Spiegel, 2015; Tamayo et al., 2020). Uncertainties are calculated by generating 1000 clones from the astrometry error fits assuming a normal distribution.

For mass estimation and event classification, it is necessary to calibrate the light curve. Using the visual magnitude of the same reference stars as in astrometry, we perform aperture photometry by subtracting the local background of each one. In this way, a logarithmic fit is conducted to relate pixel values with magnitudes. We correct the atmospheric extinction and calculate the absolute magnitude of the meteor (as observed at 100 km at the zenith).

The pre-atmospheric velocity is a critical quantity for orbit estimation and cannot be directly measured by optical devices. It is necessary to derive it from the distance traveled, for which a smooth function fit of the observed points is usually performed. For this purpose, we apply the function proposed by Whipple and Jacchia (1957) that allows the velocity to be obtained straightforwardly from its derivative. However, for high-altitude grazing meteors, this model does not perform properly as it cannot represent the velocity end. What is expected for the atmospheric entry of a meteoroid with these characteristics is a non-appreciable deceleration. For that reason, we assume that, within the error margins of the measurements, the pre-atmospheric and terminal velocities are virtually the same as a first approximation. Nevertheless, as we do not adjust the trajectory for the influence of gravity, we opt to analyze the initial third of the observed data points, conducting a linear fit with the mean value as the most likely velocity. The standard deviation of the fit serves as a measure of velocity uncertainty. As the entire trajectory can be used for velocity estimation without applying a deceleration model, this results in a smaller margin of error than expected for regular meteor velocity estimation from optical observations (Egal et al., 2017).

Assuming the radiated energy by the meteor is proportional to the loss of kinetic energy in the form of mass loss (Ceplecha, 1966), which is only theoretically valid for atmospheric flight with no deceleration (Gritsevich and Koschny, 2011), the initial meteoroid mass can be computed from

$$m_0 = \int \frac{2}{\tau(v)v^2} I(t)dt, \tag{1}$$

where τ is the luminous efficiency, v is the velocity, t is the time, $I = I_0 10^{-0.4M}$ is the radiated energy, $I_0 = 1300$ W is the zero-magnitude radiant power for high-speed meteors (Weryk and Brown, 2013), and M the absolute magnitude. The luminous efficiency in percent is taken from Ceplecha and McCrosky (1976): $\log \tau = -1.51 + \log v$ when $v \geq 27$ km s^{-1}. However, Borovička et al. (2022) note that contemporary luminous efficiency models lead to ~7 times less mass for velocities above 27 km s^{-1}, so our initial meteoroid mass may be overestimated by one order of magnitude. For example, using the Revelle and Ceplecha (2001) updated model where $\ln \tau = -1.53 + \ln v$ for $v \geq 25.372$ km s^{-1}, larger average luminous efficiency of are achieved.

Following Ceplecha and McCrosky (1976), meteors can be classified according to the so-called P_E criterion:

$$P_E = \log \rho_e - 0.42 \log m_0 + 1.49 \log v_\infty - 1.29 \log \cos z_R, \tag{2}$$

where ρ_e is the air density at terminal height, v_∞ is the pre-atmospheric velocity, and $\cos z_R$ is the apparent radiant zenith distance.

A more physical, dimensionless form of this criterion exists (Moreno-Ibáñez et al., 2020), however, as the analyzed event presents challenges in uniquely determining their atmospheric flight parameters, we turn to the original PE criterion form. From the classical third-order system describing the meteor body deceleration, numerous efforts have been made to define a height-velocity relation (Kulakov and Stulov, 1992; Gritsevich and Stulov, 2006; Gritsevich, 2007, 2008, 2009; Turchak and Gritsevich, 2014; Lyytinen and Gritsevich, 2016; Sansom et al., 2019a; Boaca et al., 2022; Peña-Asensio et al., 2023). Following these works, the dynamics of a meteor can be characterized from the analytical solution using two dimensionless parameters, namely the ballistic coefficient α and the mass loss parameter β. It is possible to express α in terms of the meteoroid bulk density ρ_m, the pre-atmospheric shape factor A_0, the drag coefficient c_d, the atmospheric density at the sea level ρ_0, the height of the homogeneous atmosphere $h_0 = 7.16$ km, the meteoroid mass m, and the slope of the trajectory with the horizon γ:

$$\alpha = \frac{1}{2} \frac{c_d A_0 \rho_0 h_0}{m_0^{1/3} \rho_m^{2/3} \sin \gamma}. \tag{3}$$

Assuming that the ablation of the body due to its rotation is uniform over the entire surface of the meteoroid (Bouquet et al., 2014), the mass loss parameter can be calculated directly from the ablation coefficient σ and the entry velocity:

$$\beta = \frac{1}{6} \sigma v_\infty^2. \tag{4}$$

We selected a uniformly distributed range of values for the ablation coefficient between 0.014 s^2 km^{-2} and 0.042 s^2 km^{-2} suitable for a rocky body based on both the classical single-body ablation and contemporary mass-loss models (Ceplecha et al., 1998; Vida et al., 2018).

Due to the high altitudes and velocities of the atmospheric flight with an enhanced mass loss under the condition of minimal deceleration, standard dynamical fits, such as $\alpha - \beta$, may not perform properly as they are often organized as a function of velocity and are not primarily intended for high-height grazers, that is, for non-decelerating flights. Nevertheless, we can use the asymptotic form of the solution obtained to describe meteor trajectories at large values of the mass loss parameter given the formal fulfillment of the condition $\ln(2\alpha\beta) < h_e/h_0 < \infty$, where h_e is the end (terminal) height (Stulov, 1997, 1998; Gritsevich and Popelenskaya, 2008; Stulov, 2004; Moreno-Ibáñez et al., 2015). To account for the possible change in velocity at the end of the luminous trajectory, we use the latest modification of this solution (Moreno-Ibáñez et al., 2015; Gritsevich et al., 2016; Moreno-Ibáñez et al., 2017):

$$v_{e'} = v_\infty \left(\frac{\ln(1 - 2\alpha\beta e^{-h_e/h_0})}{\beta} + 1 \right)^{1/2}. \tag{5}$$

Using *FireOwl* analysis software (Visuri et al., 2020; Visuri and Gritsevich, 2021), a Finnish Fireball Network tool that performs numerical integration of the meteoroid trajectory (Moilanen et al., 2021; Kyrylenko et al., 2023), we recompute and contrast all the results. Finally, we check the dynamic association with some meteoroid stream or parent body by means of the well-known D_D orbital dissimilarity criterion proposed by Drummond (1981).

3. Results

On October 23, 2022, at 19:38:34 (UTC), a very fast grazing meteor, hereafter FH1, flew through the sky of Finland and terminated over the Gulf of Bothnia. The event was observed by 3 stations of the Finnish Fireball Network (FFN) (Gritsevich et al., 2014; Trigo-Rodríguez et al., 2015; Lyytinen and Gritsevich, 2016; Visuri and Gritsevich, 2021; Moilanen et al., 2021) and 1 image observation from the public: Nyrola (Sony IMX291; 1280 × 720 px; 4 mm f/0.95), Tampere (Hikvision DS-2CD2T87G2-L; 3840 × 2160 px; 2.8 mm f/1.0), Vaala (Watec

Table 1
Longitude, latitude, and altitude of the station recording the FH1 meteor.

Station	Lon. (°)	Lat. (°)	Alt. (m.a.s.l.)
Nyrola	25.5097	62.3425	203
Vaala	26.7317	64.3917	130
Tampere	23.7931	61.5119	171
Sastamala	23.0024	61.3826	63

902H; 768 × 576 px; 3.8 mm f/0.8), and Sastamala (NIKON D750; 6016 × 4016 px; 14 mm f/4.0). These observations have been used in this study (Table 1). Fig. 1 shows two blended images of FH1 from the videos recorded by the Sastamala and Nyrola stations.

The luminous phase of FH1 started at an altitude of 126.55 ± 0.03 km (24.3104 ± 0.0008°E, 63.6677 ± 0.0002°N), traveling a distance of 409.47 ± 0.09 km until ablation ended at 112.60 ± 0.04 km altitude (18.558 ± 0.002°E, 61.2358 ± 0.0005°N). The flight angle with respect to the local horizon (i.e., the slope) was 3.588 ± 0.013°, with an azimuth of 229.915 ± 0.007° (zero being north and positive in clockwise direction). Fig. 2 shows the 3D scaled atmospheric flight reconstruction. The geocentric radiant, namely the corrected meteor anti-apex, is calculated outside of the gravitational influence field of the Earth and the Moon (at 10 times the Earth's Hill sphere), being the right ascension $\alpha_R = 117.160 \pm 0.009°$ and the declination $\delta_R = 19.444 \pm 0.020°$. The best convergence angle between the observations is ~50° (for Sastamala and Vaala stations), where plane intersections with angles smaller than 5° are excluded (only for Sastamala and Tampere stations). Table 5 in the Appendix shows the position vectors of the initial and final points of FH1's luminous path in the Earth-centered Earth-fixed coordinate system, as recorded by each of the four stations.

Fig. 3 shows the apparent point-to-point velocities, together with the fitted (73.7 ± 0.6 $km\,s^{-1}$) and the parabolic velocity threshold for this specific atmospheric trajectory (~73 $km\,s^{-1}$). For 0.2 s intervals, Nyrola detection has 71% of all instant velocity measurements above this threshold, while for Vaala it is 64%. Nyrola and Vaala stations record at 25 fps, Tampere at 2.5, and Sastamala is an image of 5 s of exposure. Note that the apparent dispersion of the point-to-point velocities depends on the time interval selected and, paradoxically, the smaller the interval, the greater the dispersion, but the more accurate the final result. In the Appendix, Tables 6 and 7 offer the detected positions of FH1 for each frame, represented in a horizontal coordinate system comprising azimuth and elevation.

We are aware that the plane intersection method may not be appropriate for long-duration grazing events (Borovicka and Ceplecha, 1992; Sansom et al., 2019b; Shober et al., 2020). Still, for this work, the approach described above is sufficient given the high velocity, brief duration (5.56 s), negligible atmospheric drag, and no dark flight calculations are required as no terminal mass is expected. Nonetheless, utilizing the fundamental equations of motion, we calculate the descent of an object due to gravitational acceleration under these conditions to be 147 m.

From the inbound velocity, we estimate the heliocentric osculating orbital elements at impact to be the following: semi-major axis $a = -8 \pm 5$ au, eccentricity $e = 1.07 \pm 0.06$, inclination $i = 177.18 \pm 0.04°$, the longitude of the ascending node $\Omega = 30.10390 \pm 0.00010°$, argument of periapsis $\omega = 16.1 \pm 0.8°$, and true anomaly $f = 343.9 \pm 0.8°$. The orbit shows no close encounters with any planets. Fig. 4 illustrates the obtained heliocentric hyperbolic orbit.

Fig. 5 shows the meteoroid absolute magnitude for every frame from Nyrola and Vaala stations, which are in good agreement with each other. FH1 curve light has a mean luminous efficiency of $\tau = 2.278 \pm 0.018\%$, a peak brightness of $M = -3.0 \pm 0.5$, and yields a photometric initial mass of $m = 1312 \pm 50$ g. Using the Revelle and Ceplecha (2001) updated model yields an average luminous efficiency of 15.96 ± 0.13%. Note that the meteoroid underwent a smooth and gradual ablation without any flares or catastrophic disruption, resulting in the absence of saturated pixels in all recordings.
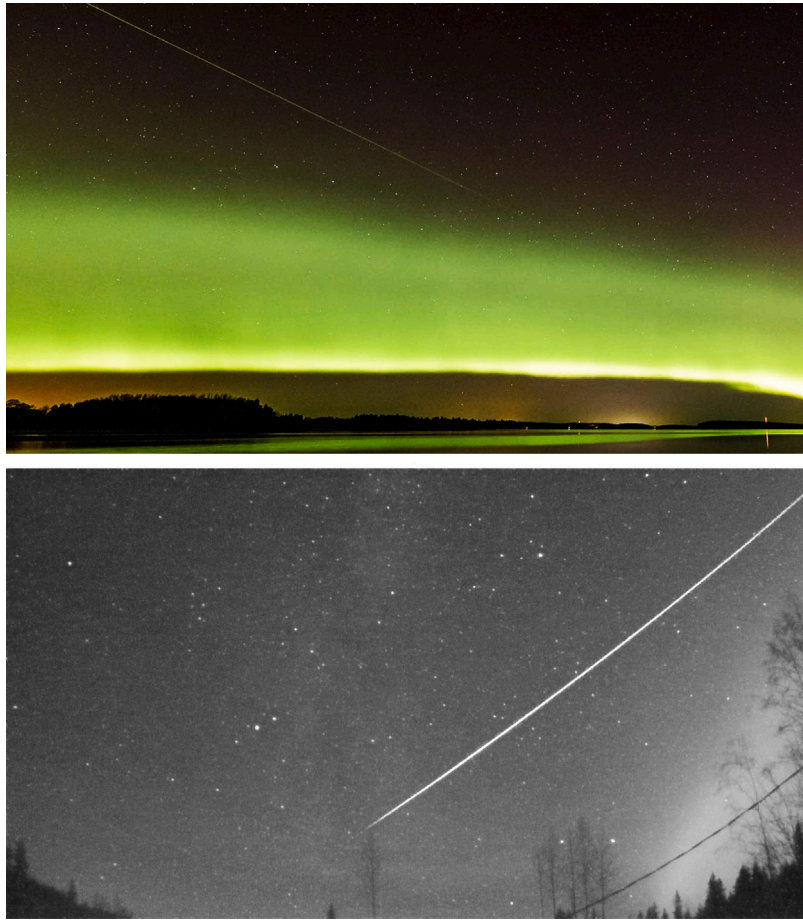
Fig. 1. Blended image of the FH1 videos recorded by Sastamala station with (top) and Nyrola station (bottom). The green illuminated area is an aurora borealis. (For interpretation of the references to color in this figure legend, the reader is referred to the web version of this article.)
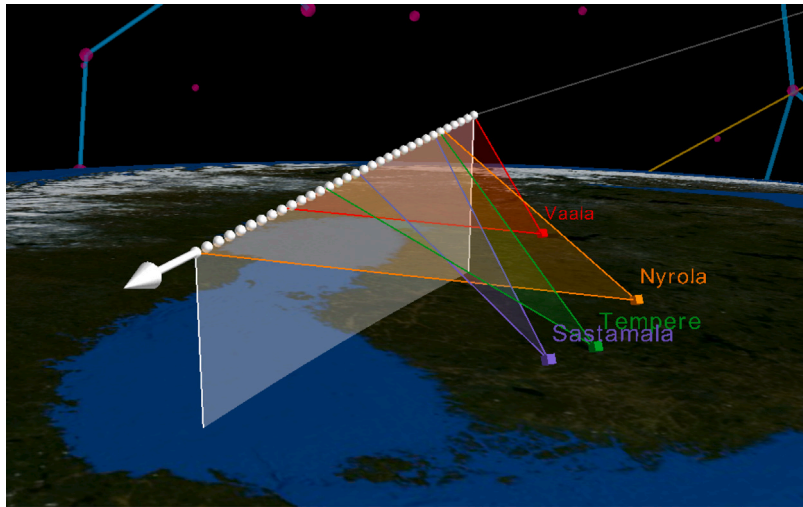

Fig. 2. 3D scaled atmospheric flight reconstruction of the FH1 meteoroid by using the Python software *3D-FireTOC*.

For FH1 meteor we obtain $P_E = -4.173 \pm 0.009$. Ceplecha and McCrosky (1976) classified meteors as type I when $P_E > -4.6$, which Ceplecha et al. (1998) assigned to ordinary chondrites. Note that the photometric mass used for P_E classification must be computed using luminous efficiency from Ceplecha and McCrosky (1976) in Eq. (2). The obtained value is in good agreement with our estimated luminous efficiency as Revelle and Ceplecha (2001) found that asteroidal fireballs should be around 5.57% and 1.35% for carbonaceous chondrite-like

fireballs. This is consistent also with similar works (Subasinghe et al., 2017; Drolshagen et al., 2021a,b). In any case, the FH1 meteoroid has a consistency equal to or greater than ordinary chondrites, tending towards high-strength materials.

Conservatively, taking an asteroid-like bulk density of 3700 kg m^{-3}, we compute an initial meteoroid diameter of 8.75 ± 0.12 cm, which in contrast may be 4.59 ± 0.06 cm in diameter based on modern luminous efficiency models. Given the inferred meteoroid size and bulk density,
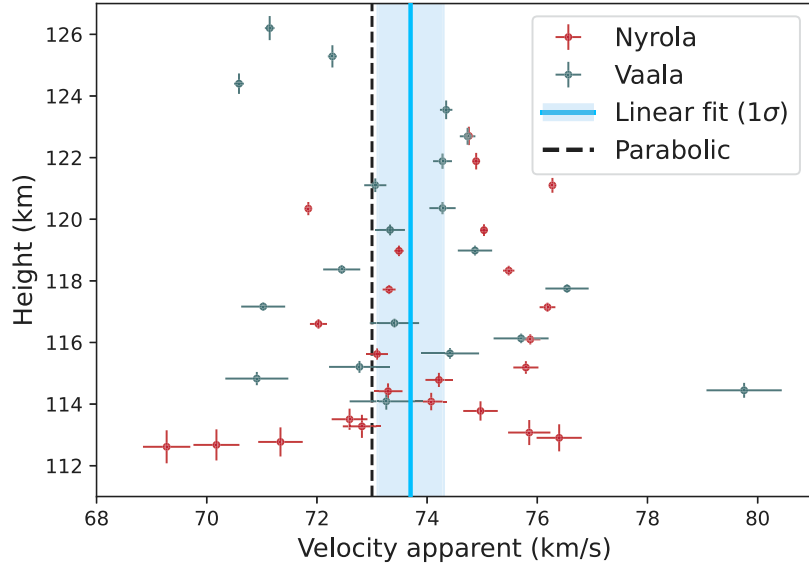
Fig. 3. Apparent velocity points of FH1 derived from Nyrola and Vaala observations computed at intervals of 0.2 s, fitted velocity, and the parabolic threshold. The error bars are multiplied by a factor of 10. (For interpretation of the references to color in this figure legend, the reader is referred to the web version of this article.)
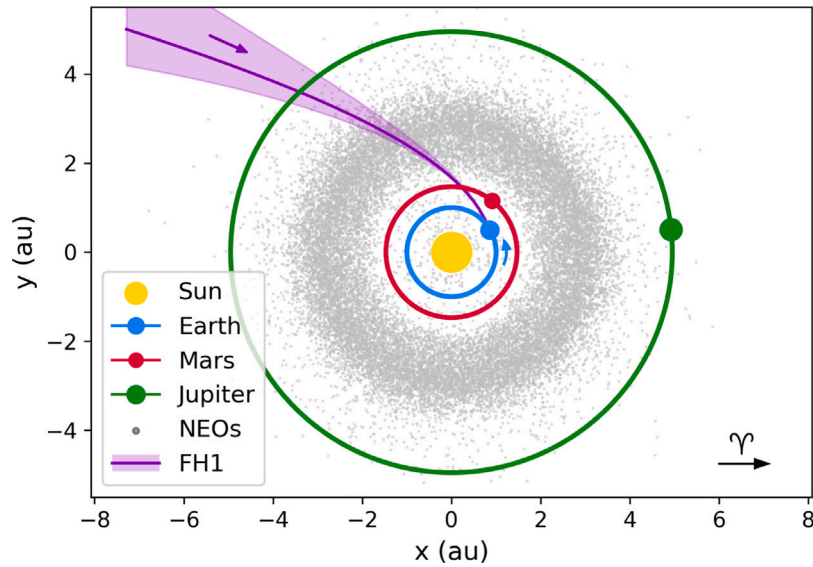

Fig. 4. Osculating heliocentric orbit of the FH1 meteoroid (J2000). The arrow at the bottom right shows the direction to the point of the vernal equinox.

an asteroidal origin seems likely (Blum et al., 2006; Trigo-Rodríguez and Llorca, 2006), although it could also be compatible with rocky pebbles ejected by cometary disintegration during inner solar system trips (Trigo-Rodríguez and Blum, 2022). From Eq. (3), we obtain a value of α of 444 ± 4 or 855 ± 7 depending on the initial photometric mass estimates previously calculated, and $\beta = 25 \pm 7$, far away from being a meteorite-dropper event (Gritsevich et al., 2012; Sansom et al., 2019a; Boaca et al., 2022). Eq. (5) yields a velocity decrease over 5 m s^{-1} and 10 m s^{-1}, which is below the resolution of the measurements and within the uncertainty margin estimated for the velocity along the flight.

We corroborate with the *FireOwl* pipeline that an asteroid-like meteoroid with no catastrophic disruption and the estimated characteristics would behave in agreement with the observations. However, differences between compositions are almost marginal as the projectile experiences a low air drag during its ~5.56 s of flight. Therefore, on this occasion, the dynamic models cannot provide conclusive results concerning the meteoroid density.

The two candidates are the Taurids swarm and the comet P/2015 A3, with a $D_D = 0.160$ and $D_D = 0.177$, respectively. These values are well above the typically accepted threshold (Galligan, 2001), so this event is definitely not associated with any known parent body or meteoroid stream.
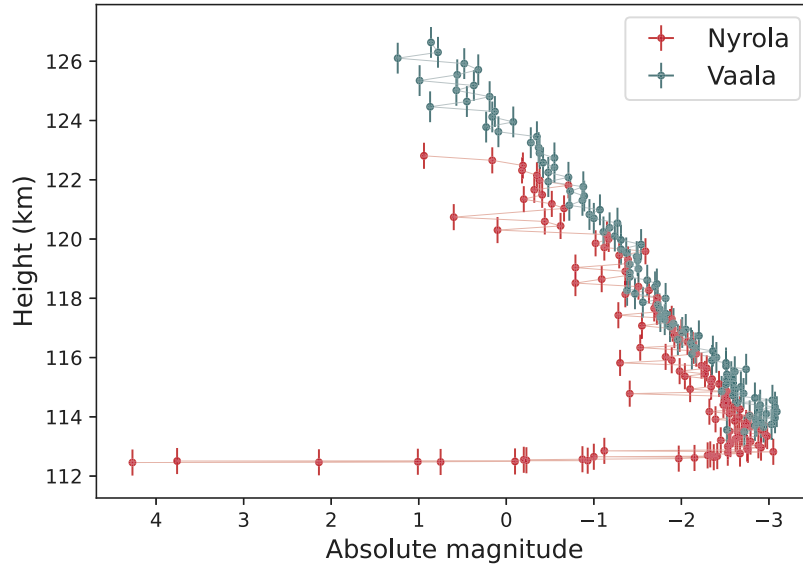
Fig. 5. Photometry of FH1 from Nyrola and Vaala stations. The mean uncertainty of the magnitude is 0.44 and 0.55 respectively. (For interpretation of the references to color in this figure legend, the reader is referred to the web version of this article.)

In summary, FH1 was a non-cometary centimeter-sized meteoroid in an inbound retrograde likely hyperbolic orbit lying almost on the ecliptic plane. It exhibits no close encounter with any known planet and a velocity excess at impact of ∼0.7 km s⁻¹ with respect to the barycenter of the solar system. Photometry of the meteor phase yields an asteroid-like (or higher) bulk density. FH1 is the first likely hyperbolic event detected by the FFN since the beginning of the year 2004, with over 2000 manually analyzed meteors. All computed parameters can be found in Table 2.

4. Discussion

The distinctive attributes of FH1, primarily its remarkably high eccentricity, could conceivably prompt conjectures regarding its interstellar origin. Notably, such speculations have been posited recently in the context of certain hyperbolic fireball events cataloged in the CNEOS database. However, a critical observation emerges when analyzing orbital inclination, which appears as a key indicator that urges to exercise caution before leaping to interstellar suppositions. We need first to investigate more plausible scenarios, including the possibility that these intriguing projectiles are either indigenous to our solar system, subject to measurement inaccuracies, or potentially subjected to gravitational accelerations.

In this section, due to the similarity with FH1, we discuss the possible interstellar origin of some CNEOS fireballs considering their uncertainties from events detected independently by ground-based stations. Additionally, we put forth the hypothesis that hyperbolic Earth impactors may be celestial bodies native to our solar nebula, which have been perturbed by close encounters with massive objects. More precisely, we propose that IM2's trajectory aligns exceptionally well in time and direction with the Scholz system fly-by when considering an overestimated velocity.

4.1. CNEOS 'interstellar' fireballs

As of October 2023, the CNEOS public database includes ∼956 fireballs starting from 1988. Among them, 6 events have hyperbolic orbits (see Table 3). These interstellar candidates have orbital inclinations lower than 25° (with an average of $12 \pm 9°$). As interstellar interlopers may originate from any part of the sky, the expected inclination should be an isotropic probability density function, which follows a sinusoidal distribution (Engelhardt et al., 2017) and, therefore, is uniform in

Table 2
Atmospheric flight, photometric, physical, and heliocentric orbital (J2000) computed parameters of FH1 grazing meteor. The values with two results correspond to the luminous efficiency models considered: Ceplecha and McCrosky (1976) on the left and Revelle and Ceplecha (2001) on the right.

Parameter		Value
Reference time (UTC)	t_0	2022-10-23 19:38:34
Velocity (km s⁻¹)	v_∞, v_0, v_e	73.7 ± 0.6
Initial latitude (°)	φ_0	63.6677 ± 0.0002N
Initial longitude (°)	λ_0	24.3104 ± 0.0008E
Initial height (km)	h_0	126.55 ± 0.03
Final latitude (°)	φ_e	61.2358 ± 0.0005N
Final longitude (°)	λ_e	18.558 ± 0.002E
Final height (km)	h_e	112.60 ± 0.04
Duration (s)	Δt	5.56
Length (km)	Δl	409.47 ± 0.09
Slope (°)	γ	3.588 ± 0.013
Azimuth (°)	A	229.915 ± 0.007
Peak brightness	M	−3.0 ± 0.5
Luminous efficiency (%)	τ	2.278 ± 0.018 | 15.96 ± 0.13
Ablation coef. (s² km⁻²)	σ	0.014 | 0.042
Initial phot. mass (g)	m_0	1312 ± 54 | 187 ± 7
P$_E$ criterion	P_E	−4.173 ± 0.009
Meteoroid density (kg m⁻³)	ρ_m	3700
Initial diameter (cm)	D	8.75 ± 0.12 | 4.59 ± 0.06
Geo. velocity (km s⁻¹)	v_R	72.7 ± 0.6
Geo. radiant (RA) (°)	α_R	117.160 ± 0.009
Geo. radiant (Dec) (°)	δ_R	19.444 ± 0.020
Hyp. excess (km s⁻¹)	Δ_v	∼0.7
Hel. velocity (km s⁻¹)	v_H	43.0 ± 0.6
Semi-major axis (au)	a	−8 ± 5
Eccentricity	e	1.07 ± 0.06
Inclination (°)	i	177.18 ± 0.04
Long. of the asc. node (°)	Ω	30.10390 ± 0.00010
Argument of periapsis (°)	ω	16.1 ± 0.8
Periapsis distance (au)	q	0.9748 ± 0.0008
True anomaly (°)	f	343.9 ± 0.8
Ballistic coef.	α	444 ± 4 | 855 ± 7
Mass-loss parameter	β	25 ± 7
Deceleration (m s⁻²)	a	0.94 ± 0.01 | 1.817 ± 0.015

$\cos i$. This implies that the random likelihood that n orbital inclinations fulfill $| i | \le \theta°$ where $i \in [-\pi/2, \pi/2]$ is $(1 - \cos\theta)^n$. Consequently, the orbits of 1I/'Oumuamua and 2I/Borisov had a likelihood of being lower than $| -58° |$ (the largest inclination which is 1I/Omumuamu's) of ∼22%. By comparison, the likelihood of detecting six interstellar objects with inclination orbits smaller than 25° is ∼0.00007%. This

Table 3
CNEOS hyperbolic fireballs with geocentric radiant, heliocentric velocity, semi-major axis, eccentricity, and orbital inclination.

Date (UTC)	α_R (°)	δ_R (°)	V_h (km s^{-1})	a (au)	e	i (°)
2022-07-28 01:36:08	276.5	14.8	46.9	−1.98	1.44	23.47
2021-05-06 05:54:27	62.5	12.2	44.1	−2.64	1.15	6.05
2017-03-09 04:16:37 (IM2)	170.6	34.1	50.1	−1.22	1.57	24.03
2015-02-17 13:19:50	339.3	−9.6	44.0	−1.45	1.10	1.12
2014-01-08 17:05:34 (IM1)	88.9	13.3	61.1	−0.46	2.42	10.05
2009-04-10 18:42:45	107.8	4.5	45.5	−1.91	1.33	6.52

Table 4
Comparison of 17 fireballs detected by USG sensors and published on CNEOS website with independent ground-based analysis. The geocentric radiant in right ascension and declination, the entry velocity, the radiant position angle deviation, and the velocity deviation are shown. The papers used as a reference are listed in the last column. Some of the geocentric parameters have been calculated from the apparent atmospheric data.

Event	Date (UTC)	α_R^{USG} (°)	δ_R^{USG} (°)	υ_e^{USG} (km s^{-1})	α_R^{REF} (°)	δ_R^{REF} (°)	υ_e^{REF} (km s^{-1})	Δ_R (°)	$\Delta\upsilon_e$ (%)	Reference
2008 TC3	2008-10-07 02:45:45	351.6	9.06	13.3	316.8	7.2	12.42	34.49	7.09	Scheirich et al. (2010)
Buzzard Coulee	2008-11-21 00:26:40	184.8	50.8	12.9	300	75	18.6	47.24	30.65	Milley (2010)
Kosice	2010-02-28 22:24:47	114.5	33.5	15.1	114.3	29	15	4.5	0.67	Borovička et al. (2013b)
Chelyabinsk	2013-02-15 03:20:21	334.5	−1.5	18.6	328.28	0.28	19.03	6.47	2.26	Borovička et al. (2013a)
Kalabity	2015-01-02 13:39:11	53.8	33.5	18.1	64.3	51.7	15.4	19.73	17.53	Devillepoix et al. (2019)
Romania	2015-01-07 01:05:59	118.7	6.1	35.7	113.8	10.13	27.76	6.31	28.6	Borovička et al. (2017)
Sariçiçek	2015-09-02 20:10:30	61.1	45.2	21.1	264.8	59.4	13.0	73.6	62.31	Unsalan et al. (2019)
Baird Bay	2017-06-30 14:26:45	273.6	−16.1	15.2	272.14	−12.5	15.1	3.87	0.66	Devillepoix et al. (2019)
Crawford Bay	2017-09-05 05:11:27	203.7	1.8	14.7	205.12	3.13	16.5	1.94	10.91	Hildebrand et al. (2018)
2018 LA	2018-06-02 16:44:12	248.7	−9.7	11.8	244.19	−10.32	12.375	4.48	4.65	Jenniskens et al. (2021)
Ozerki	2018-06-21 01:16:20	310.6	44.5	14.4	307.51	43.11	14.9	2.63	3.36	Kartashova et al. (2020)
Viñales	2019-02-01 18:17:10	325.4	−42.8	16.3	324.72	−41.43	16.9	1.46	3.55	Zuluaga et al. (2019)
2019 MO	2019-06-22 21:25:48	217.2	−16.1	9.6	237.3	−15.6	9.3	19.33	3.23	JPL Horizons (2023)
Flensburg	2019-09-12 12:49:48	183.1	−21.3	14.6	183.5	−18.55	14.77	2.78	1.15	Borovička et al. (2021)
Novo Mesto	2020-02-28 09:30:34	332	2.0	21.5	330.92	2.32	22.098	1.13	2.71	Vida et al. (2021)
Ådalen	2020-11-07 21:27:04	359.2	47.3	12.4	358.1	47.6	13.5	0.8	8.15	Kyrylenko et al. (2023)
2022 EB5	2022-03-11 21:22:46	157.5	38.1	13.2	157.0	37.6	13.0	0.64	1.54	JPL Horizons (2023)

is without considering that all 6 events are in prograde orbits, which should be expected in the 50% of extra-solar visitors and would further reduce the likelihood. Therefore, multiple options can be inferred: there are shortcoming data in the CNEOS database, these hyperbolic fireballs belonged to our solar system, or they came from sources with a directional bias.

As the error bars are not provided by USG sensors, it is necessary to narrow down the uncertainties and determine the frequency of spurious data in the database. Devillepoix et al. (2019) reported that CNEOS fireball radiants are off for most events, sometimes by only a couple of degrees but other times as much as 90°. They compared the radiants of 9 events recorded simultaneously by ground-based stations and found that the velocity vector of 4 of them was incorrectly measured by the USG sensors: Buzzard Coulee (2008-11-21 00:26:44), 2008 TC3 (2008-10-07 02:45:45), DN150102 - Kalabity (2015-01-02 13:39:11), and Crawford Bay (2017-09-05 05:11:27). As we calculate a different radiant for Crawford Bay event based on CNEOS data and, as pointed in Peña-Asensio et al. (2022), 2008 TC3 was missing a minus sign in the z velocity component, we decide to recompute the mean radiant position and velocity deviations of CNEOS fireballs including also the recent independently analyzed events Sariçiçek (2015-09-02 20:10:30) (Unsalan et al., 2019), Ozerki (2018-06-21 01:16:20) (Maksimova et al., 2020; Kartashova et al., 2020), Viñales (2019-02-01 18:17:10) (Zuluaga et al., 2019), 2019 MO (2019-06-22 21:25:48) (JPL Horizons, 2023), Flensburg (2019-09-12 12:49:48) (Borovička et al., 2021), Novo Mesto (2020-02-28 09:30:34) (Vida et al., 2021), Ådalen (2020-11-07 21:27:04) (Kyrylenko et al., 2023), and 2022 EB5 (2022-03-11 21:22:46) (JPL Horizons, 2023).

From the comparison of independently analyzed events presented in Table 4, it is found that the CNEOS radiants have a mean deviation of $21.3 \pm 43.2°$ in right ascension and $4.8 \pm 6.8°$ in declination, and a mean entry velocity deviation of $11.1 \pm 15.6\%$. It can be deduced from the standard deviations that the errors do not follow a normal distribution, as these distributions strongly depend on the relative geometry of the sensor and the fireball.

Eliminating the fireballs that appear as outliers based on the radiant position and velocity errors (2008 TC3, Buzzard Coulee, Kalabity, Romania, Sariçiçek, 2019 MO), deviations become Gaussian where the radiant would be reduced to 1.9° in right ascension and 1.7° in declination, and a 3.6% deviation in velocity, which is the scenario we assume for the study of the CNEOS fireballs. Therefore, this assumption remains valid solely under the condition that the hyperbolic CNEOS events are part of the same distribution as the events characterized by elliptical orbits in Table 4. Hence, if these events are indeed outliers, the presented results here should be ignored. Consequently, 65% of CNEOS events provide measurements accurate enough for a rough estimation of heliocentric orbits. However, this also implies that the results for two out of the six hyperbolic fireballs will be inaccurate, rendering these estimated errors inapplicable. Note that there is a lack of a significant correlation between the velocity error and the actual velocity value. When a linear fit is performed, it yields a coefficient of determination as low as 0.027. In principle, we should not assume that the faster hyperbolic ones will necessarily exhibit larger errors

These hyperbolic events, 2009-04-10 18:42:45, 2014-01-08 17:05:34 (IM1), 2017-03-09 04:16:37 (IM2), and 2021-05-06 05:54:27, appear to be somehow clusterized. The geocentric radiants of these 4 fireballs are suspiciously distributed around the Gemini constellation with an average radiant distance to the constellation center point of 34.2°. We check the likelihood that 4 out of 6 randomly selected events from the CNEOS database (the 255 fireballs analyzed in Peña-Asensio et al. (2022)) have a lower mean distance value to Gemini (10,000 draws). We find that these 4 hyperbolic events represent 1.7σ with respect to the mean, which denotes a probability of 6.9% having occurred by chance (see Fig. 6). From a completely isotropic radiant distribution, the probability of having obtained a smaller distance for 4/6 events is 4.3%. However, this does not strictly imply they are associated with each other as the anisotropic radiant distribution could be explained as well by both observational bias and solar system induced dynamics.
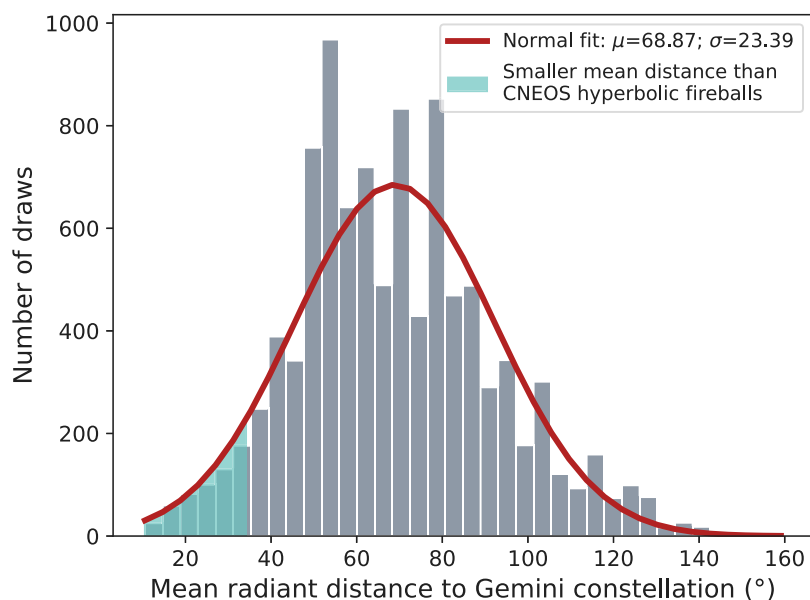
Fig. 6. Result of randomly selecting 6 CNEOS events and computing the mean minimum distance to the Gemini constellation center of 4 of them. The calculation is repeated 10,000 times. In cyan color are shown the draws with equal or smaller distances than the 6 CNEOS hyperbolic events. The fit to a Gaussian distribution is shown in red. (For interpretation of the references to color in this figure legend, the reader is referred to the web version of this article.)

4.2. The massive objects fly-by hypothesis

Not all gravitationally unbound objects from our solar system are necessarily interstellar interlopers. There are different mechanisms capable of accelerating objects native to our solar nebula into hyperbolic orbits. Some of them are the secular perturbations induced by the Galactic disk or fly-by impulsive interaction of massive extra-solar bodies (Fouchard et al., 2011; Królikowska and Dybczyński, 2017). Furthermore, close encounters with the Sun or giant planets may result in an inbound excess velocity, although these are not frequent enough to explain the observed hyperbolic meteor orbits (Hajduková et al., 2014, 2019). Mercury has also been identified as a possible efficient producer of hyperbolic projectiles to Earth (Wiegert, 2014). Other exotic hypotheses suggest unseen stellar companions to the Sun (Davis et al., 1984) or unknown planets (Socas-Navarro, 2023) as a source of hyperbolic Earth impactors.

When the idea of the Oort cloud was introduced, i.e. a very distant region with long-period comets, it was also pointed out the existence of a mechanism to shorten their perihelia, for example, inbound hyperbolic injection produced by passing stars (Oort, 1950). Indeed, recent studies suggest that stellar close encounters send accelerated bodies into the planetary zone (Dybczyński and Królikowska, 2022). Higuchi and Kokubo (2020) showed that celestial bodies of sub-stellar mass (down to approximately 0.2 Jupiter masses) possess the ability to divert Oort cloud comets into hyperbolic trajectories characterized by small eccentricity but large perihelion distance. Other stellar systems may have also their own Oort-like clouds which could induce an influx of extra-solar objects through the planetary region when approaching the Sun (Stern, 1987). The most recent stellar fly-by to our solar system was the low-mass binary star WISE J072003.20−084651.2, also known as Scholz's star (hereafter Scholz), which crossed the outer layers of the Oort cloud at 52^{+23}_{-14} kau about 70^{+15}_{-10} kya ago (Scholz, 2014; Burgasser et al., 2015; Mamajek et al., 2015).

de la Fuente Marcos et al. (2018) analyzed hyperbolic small bodies of the data provided by JPL's solar system Dynamics Group Small-Body and the Minor Planets Center (MPC) databases. They found strong anisotropies on the geocentric radiant distribution with a statistically significant overdensity of high-speed radiants towards the constellation of Gemini, which appears to be consistent in terms of time and location with the Scholz fly-by. Precisely the geocentric radiant of FH1 falls in this constellation, as well as 4 of the 6 hyperbolic fireballs from the CNEOS database that are close to Gemini or the recent Scholz motion direction.

We test the compatibility of this hypothesis by integrating backward in time the FH1 grazer and the 6 CNEOS interstellar candidates for 109,000 years to account for the estimated upper time limit of the Scholz close encounter (85,000 years). To this end, we use an orbital integrator based on a leapfrog scheme with different time steps to properly resolve the Earth-induced zenith attraction prior to the impact (Socas-Navarro, 2019). We account for the gravitational influence of the Sun, Earth, Moon, Mars, Jupiter, Saturn, Uranus, and Neptune by querying ephemerids to JPL HORIZONS system. Fig. 7 shows the apparent motion of the objects starting from their geocentric radiants for the considered time. None of the events experienced a close encounter with planets, only 2021-05-06 05:54:27 fireball passed ~5 years ago at ~3 times Hill radius from Uranus.

New results definitively dismiss the possibility that Scholz may have penetrated the dynamically active inner Oort cloud region (<20 kAU), but support the notion that it would have passed through the outer Oort cloud where objects can have stable orbits (Dupuy et al., 2019; de la Fuente Marcos and de la Fuente Marcos, 2022). Given the apparently better constrained time (~80 kya) and distance (~68 kau) for the Scholz close encounter, and its current separation from the Sun (6.80 pc), it can be computed a linear velocity with respect to the solar system barycenter of $v^* = 82.4 \pm 0.3$ km s^{-1}, which is a valid approximation for 100 kya within 2.5% accuracy (Mamajek et al., 2015). Considering the fly-by occurring at high velocity and the low mass of the Scholz system ($M_* = 165 \pm 7 \, M_{Jup}$), it appears plausible that small bodies may have been injected towards the Earth.

The meteoroid FH1 was 36 ± 18 kya ago at ~67 kau, and the IM2 object reached the same distance 14 ± 2 kya ago. The closest encounter
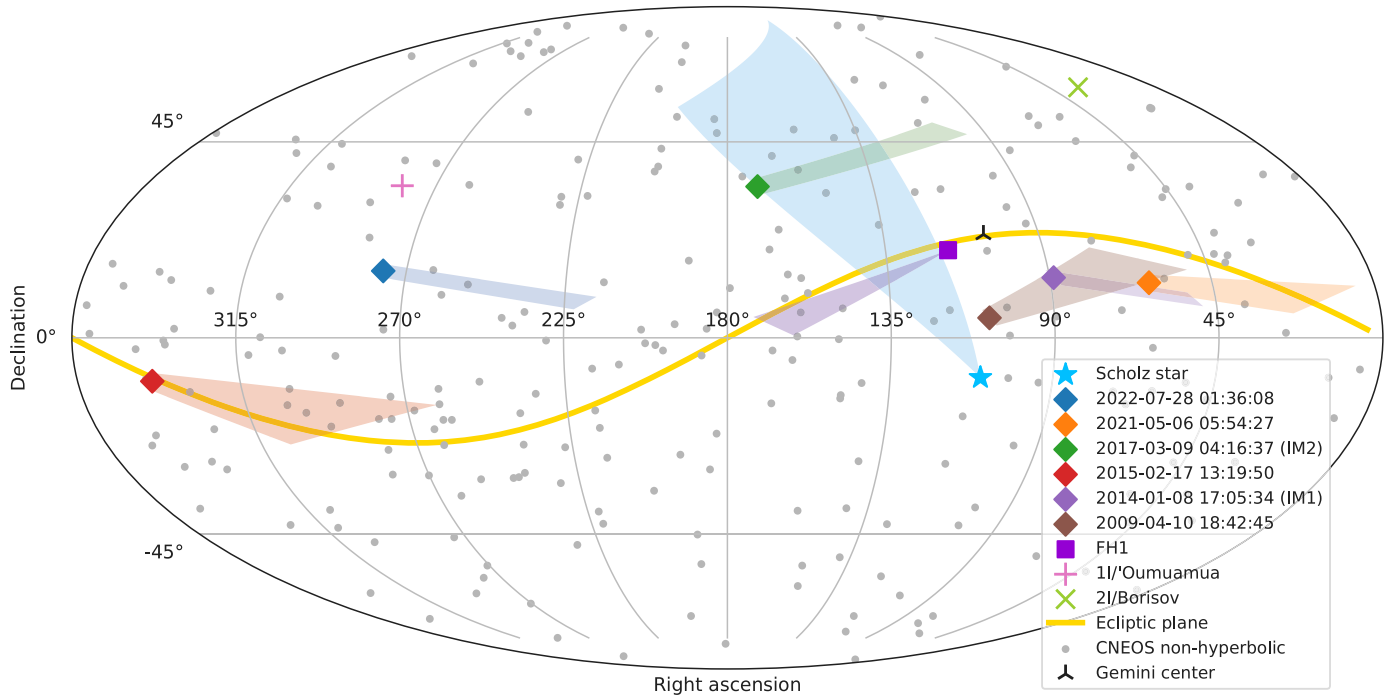
Fig. 7. Apparent motion of the objects starting from their geocentric radiants during the backward orbital integration. Scholz, FH1 grazer event, 1I/'Oumuamua (Meech et al., 2017), and 2I/Borisov (de León et al., 2020) are shown. The 6 dated events correspond to the hyperbolic fireballs in the CNEOS database and include the new mean deviation found for the 17 fireballs compared. All CNEOS non-hyperbolic events are also depicted, together with a center point of the Gemini constellation. Markers represent the radiant position at impact or at the current time in the case of Scholz. The ecliptic plane is plotted in yellow. (For interpretation of the references to color in this figure legend, the reader is referred to the web version of this article.)

found in the simulation of FH1 with the Scholz trajectory was at 39 kau, while IM2 passed at 131 kau. In spite of almost intersecting trajectories, the excess velocity of IM2 at impact (-8 km s^{-1}) causes it not to be compatible in time with the Scholz passage. Looking at Table 4, it can be seen that $\sim$18% of the events have velocity errors around 30% or more of the nominal value. If the IM2 measurement had an uncertainty of 22% it would be perfectly compatible in time with the Scholz fly-by. Velocities proximal to the parabolic limit for FH1 are consistent, both temporally and directionally, with the passage of Scholz. This consistency necessitates only a 1% reduction in Scholz's nominal velocity, a value well within the estimated range of uncertainty. Fig. 8 presents the geometric configuration of the encounter involving FH1, IM2, and Scholz.

Long-period objects can acquire excess velocity from relatively low gravitational perturbations with no need for very close encounters if they are oriented in the appropriate direction at the appropriate time. Moreover, the perturbation may not necessarily have occurred during the time of the maximum approach of Scholz, which took $\sim$21.5 kya to traverse the Oort cloud. Considering that an object is fixed in reference to the solar system barycenter, it is possible to estimate the time-integrated impulse exerted by a passing star from classical impulse approximation (Rickman et al., 2005):

$$\Delta v = \frac{2GM_*}{v^*} \left(\frac{\hat{b}_o}{b_o} - \frac{\hat{b}_*}{b_*} \right), \tag{6}$$

where G is the gravitational constant, b_o is the vector from the Oort cloud object to the Scholz closest approach, and b_* is the vector from the Sun to the Scholz closest approach.

To elucidate, consider a notional object situated at a radial distance of 39 kau beyond the point of closest approach between the Scholz star

system and the Sun, which occurs at 68.7 kau. According to Eq. (6), the interaction with the Scholz could impart a maximum velocity change of approximately 0.136 m s^{-1}. In the defined encounter geometry within the Oort Cloud, the object would need to achieve a velocity of 0.982 m s^{-1} to attain a perihelion distance of 1 au. The velocity impulse generated by the Scholz star would represent approximately 14% of the object's perigee velocity. Therefore, such a perturbation has the capacity to significantly modify the orbital parameters of a distantly located object, resulting in a highly eccentric inbound trajectory towards Earth.

Detection of exocomets and warm and cold debris belts around stars suggests the existence of Oort-like outer clouds material in other stellar systems (Marois et al., 2010; Kiefer et al., 2014). Highly eccentric evaporating comets are compatible with the metallic absorption lines observed in debris disk spectra, which may be evidence of exocomet clouds (Beust et al., 1990; Hanse et al., 2018). Hanse et al. (2018) found that 25% to 65% of the mass lost from the Oort cloud is due to objects being either injected into the planetary region or ejected into interstellar space mainly because of stellar encounters. A hypothetical Oort-like Scholz cloud should have the outer edge less distant from its center than the Sun due to its smaller mass. Assuming that both stellar systems have undergone similar processes, we can establish that the binding energies of their outer clouds of material are roughly the same and, therefore, their gravitational potential energies as well:

$$-\frac{GM_\odot m_o}{R_\odot} = -\frac{GM_* m_o}{R_*}, \tag{7}$$

where R is the distance from the objects to the star, m_o is the mass of the surrounding objects, $\odot$ subscript refers to the Sun, and $*$ to another star. Accordingly, the outer edge of the Scholz outer cloud should be scaled down as $R_* = 0.16 R_\odot$.
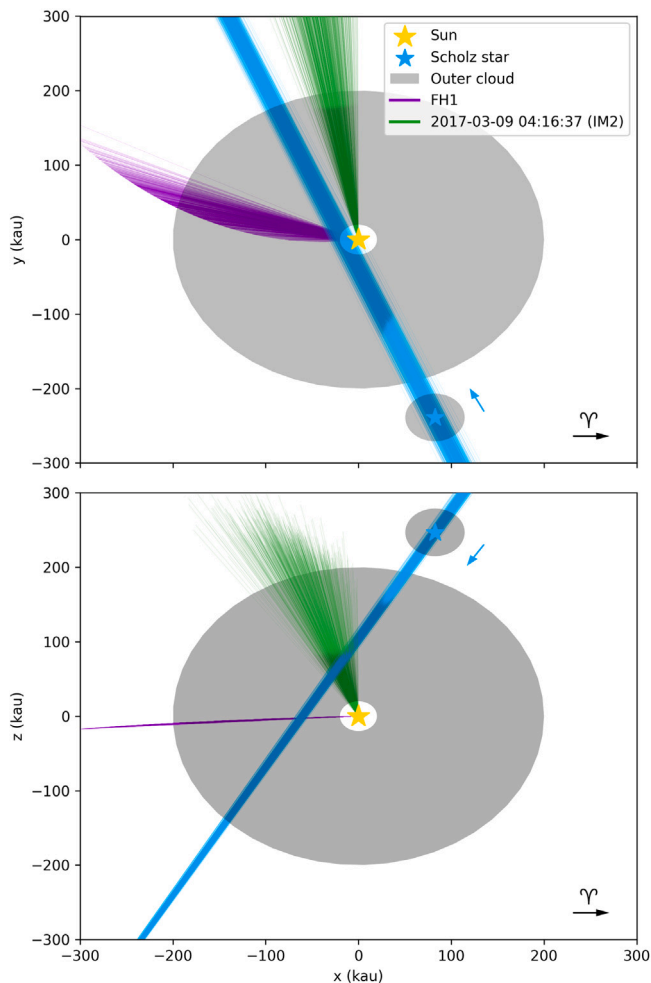
Fig. 8. Integration of clones for FH1, IM2, and Scholz. The diagram illustrates the heliocentric cartesian coordinates evolution during the encounter, including the respective outer clouds of material associated with both the Sun and Scholz. The arrow at the bottom right shows the direction to the point of the vernal equinox. (For interpretation of the references to color in this figure legend, the reader is referred to the web version of this article.)

Given that the classical outer edge of the Oort cloud is 200 kau (Dones et al., 2004), it is expected that the Scholz system has an outer cloud edge of 32 kau, close enough to the Sun for any object to be disturbed towards the planetary region during the fly-by, even more so when Scholz Hill sphere at the closest approach was 26 kau. In fact, IM2 clone trajectory traversed the path of the Scholz cloud and a considerable percentage of the clones intersected its Hill sphere path, while some FH1 clones passed at 2 Scholz Hill sphere radius. These possible injections could be facilitated by the joined effect of the Galactic disk, other passing stars interactions, and the presence of massive objects on the outskirts of the Scholz system or of our solar system. For example, the Scholz motion region passes through the zone of high probability for the putative planet 9 and multiple hyperbolic CNEOS fireballs fall around it (Batygin and Brown, 2016; Brown and Batygin, 2021; Socas-Navarro, 2023). Note that although the maximum velocity change in a fly-by is double the relative velocity of the encounter, a very massive nearly static object could redirect another with a zero net velocity change into a hyperbolic orbit due to the new geometry of the motion with respect to the central body. However, this situation would lead to slow unbound orbits, which might explain the modest impact velocity excess for many hyperbolic solar objects.

With successive data releases from Gaia, the space observatory of the European Space Agency, the identification of new stellar close encounters has been increasing. For example, in the first Gaia data release (GDR1) 2 stars (out of 300,000) were found to come within 1 pc of the Sun (Bailer-Jones, 2018), while in GDR2 were 26 stars (out of 7.2 million) passing within the same distance (Bailer-Jones et al., 2018) and 61 stars (out of 33 million) in GDR3 (Bailer-Jones, 2022). Bailer-Jones et al. (2018) inferred the present rate of stellar encounters to be 19.7 ± 2.2 per Myr within 1 pc. This implies that the Oort cloud is expected to have experienced ∼2 interloper visits in the last 80 kya. However, only one has been identified during this period of time.

We stress that as uncertainties of CNEOS data are unavailable, no definite conclusions can be established regarding IM2. Nevertheless, considering that there may be complex gravitational interactions, we claim that both FH1 and IM2 are consistent with being gravitationally accelerated impactors originating from the Oort Cloud, likely injected during Scholz's recent fly-by. Additionally, IM2 could plausibly be an object ejected from the outer cloud of the Scholz binary system. The other CNEOS hyperbolic events (if they are not outliers) possibly have experienced close encounters with massive objects (such as stars, free-floating brown dwarfs, rogue planets, sub-stellar or sub-Jovian mass perturbers, rogue planets, primordial black holes...) when traversing the Oort cloud less time ago than the Scholz passage, which in the case of a star could be supported by the current rate of stellar encounters.

5. Conclusions

We have analyzed an unusual grazing meteor (FH1) recorded in October 2022 by the Finnish Fireball Network. The cm-sized meteoroid exhibited an inbound likely hyperbolic orbit and an (at least) asteroidal consistency. Considering that its orbital plane coincides with the ecliptic and is close to the parabolic velocity limit, it seems more likely to be a perturbed Oort cloud object rather than an interstellar interloper. Within the estimated uncertainties, FH1 could be associated with the known most recent stellar encounter with our solar system, i.e., the Scholz system.

4 of the 6 hyperbolic CNEOS fireballs exhibit a statistical oddity in the geocentric radiant distribution around the Gemini constellation, an area with an overdensity of hyperbolic radiants and identified as compatible in time with the Scholz fly-by. We show statistical evidence that these events cannot really pertain to a randomly incoming interstellar population as the likelihood of their low orbital inclinations is extremely improbable compared to the expected one (with a probability of having occurred by chance of 0.00007%). Therefore, these impactors most likely belonged to our solar nebula and have been perturbed by massive objects lying on or intersecting the plane of the ecliptic. These massive objects could also form part of the Oort cloud, although this would limit the excess velocity of the projectiles.

Given the new mean uncertainties estimated in this work for CNEOS detections by benchmarking with 17 independent ground-based observations, the 2017-03-09 04:16:37 (IM2) fireball appears to be consistent with the Scholz close encounter if the velocity was overestimated by 22%, which is within the error range for ∼18% of events compared. In addition, IM2 showed a peak power in its light curve that corresponded to a dynamic pressure (i.e. aerodynamic strength) typical of iron meteorites, about ∼75 MPa, and most likely produced a recoverable metallic meteorite (Peña-Asensio et al., 2022; Siraj and Loeb, 2022b). This would inaugurate a window of opportunity for stellar archaeology sample collection with known trajectory beyond the tiny presolar grains embedded in meteorites.

If these hyperbolic impactors were interstellar visitors, it would have significant implications both for the incoming flux of extra-solar objects and for the characterization of their physical properties, which would be biased towards high-strength compositions and low inclinations. If they were Oort cloud objects, FH1 would be the second cm-sized asteroid-like observed object after Vida et al. (2023) and

IM2 the first detected iron-like body from the outermost part of our solar or another stellar system. This would provide further evidence for the massive proto-asteroid belt and Jupiter's "Grand Tack" dynamical instability scenario (Shannon et al., 2019). It would imply that the Oort cloud could currently be populated not only by weak cometary objects but also by ice-free rocky material scattered by giant planets's round trip to inner orbits.

The absence of interstellar meteorites and the low orbital inclinations of the hyperbolic projectiles studied indicate that the population of massive objects forming and crossing the Oort cloud may be larger than previously thought, injecting large meteoroids to the planetary regions. Our results reinforce the idea that passing stars or other massive objects represent a source of hyperbolic Earth impactors that must be examined in detail on a case-by-case basis before claiming the interstellar origin of any object with excess velocity.

CRediT authorship contribution statement

Eloy Peña-Asensio: Performed the analysis of FH1, The statistical study of CNEOS hyperbolic events, The investigation of the massive object close encounters hypothesis, Wrote the manuscript. **Jaakko Visuri:** Coordinated the Finnish Fireball Network efforts and supported the astrometry and atmospheric trajectory calculation of FH1. **Josep M. Trigo-Rodríguez:** Oversaw the research activity and provided scientific insights. **Hector Socas-Navarro:** Performed the N-body simulations and suggested the possible association of FH1 with Scholz's star. **Maria Gritsevich:** Clarified the issues with the dynamic model fit and contributed to the estimation of the terminal velocity. **Markku Siljama:** First identified FH1 as an interstellar candidate. **Albert Rimola:** Acquired financial support for the project leading to this publication, Supervised the work.

Declaration of competing interest

The authors declare that they have no known competing financial interests or personal relationships that could have appeared to influence the work reported in this paper.

Data availability

Data will be made available on request.

Acknowledgments

Appendix

See Tables 5–7 for observational data of FH1.

Table 5

Position vectors of the initial and final points of FH1's luminous path in the Earth-centered Earth-fixed coordinate system, as recorded by each of the four stations.

	Nyrola	Vaala	Tampere	Sastamala
X_{beg} (m)	2,684,184 ± 6	2,637,480 ± 4	2,743,469 ± 4	2,701,116 ± 3
Y_{beg} (m)	1,161,276 ± 14	1,188,673 ± 56	1,126,497 ± 7	1,151,343 ± 11
Z_{beg} (m)	5,787,091 ± 29	5,806,802 ± 26	5,762,070 ± 20	5,779,945 ± 31
X_{end} (m)	2,969,352 ± 17	2,891,289 ± 15	2,838,781 ± 2	2,800,918 ± 3
Y_{end} (m)	993,989 ± 114	1,039,782 ± 122	1,070,585 ± 21	1,092,797 ± 10
Z_{end} (m)	5,666,739 ± 24	5,699,684 ± 6	5,721,845 ± 21	5,737,825 ± 19

Table 6

Detected positions of FH1 in a horizontal coordinate system for each frame from Nyrola. The table presents the azimuth and elevation coordinates along with their corresponding frame numbers. The mean residuals from astrometry are 0.0139° for azimuth and 0.0121° for elevation.

#	Azi. (°)	Elev. (°)	#	Azi. (°)	Elev. (°)	#	Azi. (°)	Elev. (°)
11	317.3931	37.8781	51	281.3995	29.5673	91	263.1464	20.2415
12	316.2749	37.8103	52	280.7005	29.2648	92	262.8051	20.0648
13	315.3540	37.7320	53	280.0772	28.9837	93	262.5361	19.8995
14	314.1403	37.6221	54	279.4517	28.7645	94	262.2554	19.7190
15	313.1072	37.5227	55	278.8840	28.4955	95	261.9023	19.5021
16	311.9602	37.4195	56	278.2156	28.2280	96	261.6241	19.3508
17	310.8714	37.2770	57	277.6835	27.9869	97	261.3567	19.1678
18	309.8847	37.1485	58	277.0828	27.6925	98	261.1147	19.0138
19	308.7614	36.9825	59	276.4748	27.4461	99	260.8124	18.8077
20	307.8117	36.8475	60	276.0162	27.2016	100	260.5358	18.6459
21	306.6819	36.6881	61	275.4985	26.9515	101	260.2954	18.4980
22	305.7508	36.5257	62	274.9191	26.6835	102	260.0438	18.3728
23	304.6602	36.3582	63	274.3874	26.4317	103	259.7673	18.1635
24	303.5926	36.1520	64	273.8917	26.1857	104	259.4929	18.0146
25	302.6033	35.9439	65	273.3587	25.9597	105	259.2896	17.8871
26	301.5501	35.7376	66	272.8778	25.6810	106	259.0386	17.7289
27	300.6744	35.5661	67	272.3491	25.4399	107	258.8114	17.5625
28	299.6912	35.3705	68	271.8988	25.2108	108	258.5265	17.3885
29	298.7177	35.1155	69	271.4487	24.9688	109	258.3008	17.2594
30	297.7942	34.9211	70	271.0233	24.7566	110	258.0748	17.0994
31	296.9946	34.6887	71	270.5782	24.5114	111	257.8603	16.9311
32	295.9840	34.4713	72	270.0966	24.2465	112	257.6202	16.7871
33	295.1154	34.1997	73	269.6739	23.9963	113	257.3981	16.6365
34	294.3219	34.0078	74	269.2575	23.7892	114	257.1762	16.4860
35	293.4068	33.7414	75	268.8598	23.5792	115	256.9630	16.3234
36	292.5561	33.4805	76	268.4249	23.3262	116	256.7421	16.2062
37	291.7253	33.2369	77	268.0482	23.1121	117	256.5569	16.0777
38	290.9343	33.0065	78	267.6577	22.9201	118	256.3266	15.9198
39	290.0894	32.7342	79	267.2421	22.6909	119	256.1412	15.8074
40	289.3101	32.4818	80	266.8870	22.4885	120	255.9655	15.7245
41	288.5378	32.2250	81	266.4824	22.2579	121	255.7539	15.5943
42	287.7816	31.9863	82	266.1553	22.0821	122	255.5601	15.4522
43	287.0466	31.7155	83	265.7647	21.8330	123	255.3926	15.2929
44	286.1926	31.4039	84	265.4642	21.6612	124	255.2166	15.1914
45	285.4432	31.1795	85	265.1273	21.4680	125	255.0321	15.0947
46	284.7507	30.8916	86	264.7417	21.2385	126	254.8746	14.9874
47	284.0495	30.6277	87	264.4171	21.0196	127	254.7251	14.8853
48	283.3727	30.3440	88	264.1204	20.8522	128	254.5671	14.7714
49	282.7171	30.1159	89	263.7876	20.6626	129	254.4091	14.6573
50	281.9793	29.8009	90	263.4555	20.4567	130	254.2257	14.5249

Table 7

Detected positions of FH1 in a horizontal coordinate system for each frame from Vaala. The table presents the azimuth and elevation coordinates along with their corresponding frame numbers. The mean residuals from astrometry are 0.0197° for azimuth and 0.0227° for elevation.

#	Azi. (°)	Elev. (°)	#	Azi. (°)	Elev. (°)	#	Azi. (°)	Elev. (°)
1	236.5024	40.6797	37	234.6534	24.9055	73	233.8727	16.7750
2	236.4637	40.1331	38	234.6508	24.5810	74	233.8427	16.5849
3	236.4142	39.6152	39	234.6147	24.2971	75	233.8378	16.4120
4	236.3346	38.9983	40	234.5789	24.0129	76	233.8159	16.2693
5	236.2319	38.4367	41	234.5689	23.7488	77	233.8006	16.0920
6	236.2106	37.8006	42	234.5588	23.4434	78	233.8024	15.9098
7	236.0623	37.3039	43	234.5294	23.1309	79	233.8085	15.7675
8	236.0186	36.7238	44	234.4965	22.8900	80	233.7928	15.6158
9	235.9471	36.2442	45	234.4648	22.6491	81	233.7849	15.4864
10	235.9124	35.7728	46	234.4474	22.4038	82	233.7755	15.3248
11	235.8074	35.1764	47	234.4247	22.1466	83	233.7612	15.1485
12	235.7534	34.7154	48	234.3921	21.8638	84	233.7480	15.0289
13	235.7152	34.2276	49	234.3605	21.6066	85	233.7318	14.9025
14	235.6506	33.7938	50	234.3589	21.3495	86	233.7164	14.7759
15	235.5591	33.3065	51	234.3200	21.1474	87	233.6986	14.6423
16	235.5453	32.8562	52	234.2690	20.9154	88	233.7021	14.5191
17	235.5569	32.3975	53	234.2688	20.7354	89	233.6894	14.3999
18	235.4853	31.9917	54	234.2627	20.5153	90	233.6885	14.2619
19	235.4064	31.5686	55	234.2130	20.3090	91	233.6790	14.1260
20	235.3152	31.0649	56	234.2046	20.0306	92	233.6814	13.9712
21	235.2724	30.6519	57	234.1940	19.7954	93	233.6727	13.8354
22	235.2357	30.1940	58	234.2006	19.6316	94	233.6600	13.7175
23	235.1817	29.8083	59	234.1991	19.3949	95	233.6379	13.5695
24	235.1289	29.4228	60	234.1542	19.1211	96	233.6235	13.4441
25	235.0852	29.0555	61	234.1356	18.9411	97	233.6147	13.3094
26	235.0264	28.6525	62	234.1343	18.7553	98	233.6142	13.1893
27	235.0307	28.2694	63	234.0993	18.5305	99	233.6123	13.0649
28	234.9547	27.9376	64	234.0808	18.3512	100	233.6168	12.9437
29	234.9304	27.5458	65	234.0312	18.1898	101	233.6102	12.8553
30	234.9257	27.2064	66	234.0048	18.0134	102	233.6139	12.7641
31	234.8863	26.8479	67	233.9729	17.8215	103	233.5709	12.6515
32	234.8490	26.5312	68	233.9511	17.6021	104	233.5740	12.5760
33	234.7756	26.1715	69	233.9112	17.4138	105	233.5425	12.4799
34	234.7705	25.8454	70	233.8998	17.2750	107	233.5334	12.2986
35	234.7604	25.5074	71	233.8739	17.1247	108	233.4896	12.1700
36	234.7124	25.2397	72	233.8495	16.9489			

References

Almond, M., Davies, J.G., Lovell, A.C.B., 1951. The velocity distribution of sporadic meteors. I. Mon. Not. R. Astron. Soc. 111, 585. http://dx.doi.org/10.1093/mnras/111.6.585.

Almond, M., Davies, J.C., Lovell, A.C.B., 1952. The velocity distribution of sporadic meteors. II. Mon. Not. R. Astron. Soc. 112, 21. http://dx.doi.org/10.1093/mnras/112.1.21.

Bailer-Jones, C.A.L., 2018. The completeness-corrected rate of stellar encounters with the sun from the first gaia data release. Astron. Astrophys. 609, A8. http://dx.doi.org/10.1051/0004-6361/201731453, arXiv:1708.08595.

Bailer-Jones, C.A.L., 2022. Stars that approach within one parsec of the sun: New and more accurate encounters identified in gaia data release 3. Astrophys. J. Lett. 935 (1), L9. http://dx.doi.org/10.3847/2041-8213/ac816a, arXiv:2207.06258.

Bailer-Jones, C.A.L., Rybizki, J., Andrae, R., Fouesneau, M., 2018. New stellar encounters discovered in the second gaia data release. Astron. Astrophys. 616, A37. http://dx.doi.org/10.1051/0004-6361/201833456, arXiv:1805.07581.

Batygin, K., Brown, M.E., 2016. Evidence for a distant giant planet in the solar system. Astron. J. 151 (2), 22. http://dx.doi.org/10.3847/0004-6256/151/2/22, arXiv:1601.05438.

Beust, H., Lagrange-Henri, A.M., Vidal-Madjar, A., Ferlet, R., 1990. The beta pictoris circumstellar disk. X. Numerical simulations of infalling evaporating bodies. Astron. Astrophys. 236, 202.

Blum, J., Schräpler, R., Davidsson, B.J.R., Trigo-Rodríguez, J.M., 2006. The physics of protoplanetesimal dust agglomerates. I. Mechanical properties and relations to primitive bodies in the solar system. Astrophys. J. 652 (2), 1768–1781. http://dx.doi.org/10.1086/508017.

Boaca, I., Gritsevich, M., Birlan, M., Nedelcu, A., Boaca, T., Colas, F., Malgoyre, A., Zanda, B., Vernazza, P., 2022. Characterization of the fireballs detected by all-sky cameras in Romania. Astrophys. J. 936 (2), 150. http://dx.doi.org/10.3847/1538-4357/ac8542.

Borisov, G.V., Shustov, B.M., 2021. Discovery of the first interstellar comet and the spatial density of interstellar objects in the solar neighborhood. Solar Syst. Res. 55 (2), 124–131. http://dx.doi.org/10.1134/S0038094621020027.

Borovicka, J., Ceplecha, Z., 1992. Earth-grazing fireball of october 13, 1990. Astron. Astrophys. 257 (1), 323–328.

Borovicka, J., Spurny, P., Keclikova, J., 1995. A new positional astrometric method for all-sky cameras. Astron. Astrophys. 112, 173.

Borovička, J., Bettonvil, F., Baumgarten, G., Strunk, J., Hankey, M., Spurný, P., Heinlein, D., 2021. Trajectory and orbit of the unique carbonaceous meteorite Flensburg. Meteorit. Planet. Sci. 56 (3), 425–439. http://dx.doi.org/10.1111/maps.13628, arXiv:2101.02177.

Borovička, J., Setvák, M., Roesli, H., Kerkmann, J.K., 2020. Satellite observation of the dust trail of a major bolide event over the Bering sea on december 18, 2018. Astron. Astrophys. 644, A58. http://dx.doi.org/10.1051/0004-6361/202039393, arXiv:2010.13597.

Borovička, J., Spurný, P., Brown, P., Wiegert, P., Kalenda, P., Clark, D., Shrbený, L., 2013a. The trajectory, structure and origin of the Chelyabinsk asteroidal impactor. Nature 503 (7475), 235–237. http://dx.doi.org/10.1038/nature12671.

Borovička, J., Spurný, P., Grigore, V.I., Svoreň, J., 2017. The january 7, 2015, superbolide over Romania and structural diversity of meter-sized asteroids. Planet. Space Sci. 143, 147–158. http://dx.doi.org/10.1016/j.pss.2017.02.006, arXiv:1702.03968.

Borovička, J., Spurný, P., Shrbený, L., Štork, R., Kotková, L., Fuchs, J., Keclíková, J., Zichová, H., Mánek, J., Váchová, P., Macourková, I., Svoreň, J., Mucke, H., 2022. Data on 824 fireballs observed by the digital cameras of the European fireball network in 2017–2018. I. Description of the network, data reduction procedures, and the catalog. Astron. Astrophys. 667, A157. http://dx.doi.org/10.1051/0004-6361/202244184, arXiv:2209.11186.

Borovička, J., Tóth, J., Igaz, A., Spurný, P., Kalenda, P., Haloda, J., Svoreå, J., Kornoš, L., Silber, E., Brown, P., HusáRik, M., 2013b. The košice meteorite fall: Atmospheric trajectory, fragmentation, and orbit. Meteorit. Planet. Sci. 48 (10), 1757–1779. http://dx.doi.org/10.1111/maps.12078.

Bouquet, A., Baratoux, D., Vaubaillon, J., Gritsevich, M.I., Mimoun, D., Mousis, O., Bouley, S., 2014. Simulation of the capabilities of an orbiter for monitoring the entry of interplanetary matter into the terrestrial atmosphere. Planet. Space Sci. 103, 238–249. http://dx.doi.org/10.1016/j.pss.2014.09.001.

Brown, M.E., Batygin, K., 2021. The orbit of planet nine. Astron. J. 162 (5), 219. http://dx.doi.org/10.3847/1538-3881/ac2056, arXiv:2108.09868.

Brown, P.G., Borovička, J., 2023. On the proposed interstellar origin of the USG 20140108 fireball. Astrophys. J. 953 (2), 167. http://dx.doi.org/10.3847/1538-4357/ace421.

Brown, P., Wiegert, P., Clark, D., Tagliaferri, E., 2016. Orbital and physical characteristics of meter-scale impactors from airburst observations. Icarus 266, 96–111. http://dx.doi.org/10.1016/j.icarus.2015.11.022, arXiv:1511.07479.

Burgasser, A.J., Gillon, M., Melis, C., Bowler, B.P., Michelsen, E.L., Bardalez Gagliuffi, D., Gelino, C.R., Jehin, E., Delrez, L., Manfroid, J., Blake, C.H., 2015. WISE J072003.20-084651.2: an old and active M9.5 + T5 spectral binary 6 pc from the sun. Astron. J. 149 (3), 104. http://dx.doi.org/10.1088/0004-6256/149/3/104, arXiv:1410.4288.

Ceplecha, Z., 1966. Dynamic and photometric mass of meteors. Bull. Astron. Inst. Czech. 17, 347.

Ceplecha, Z., 1987. Geometric, dynamic, orbital and photometric data on meteoroids from photographic fireball networks. Bull. Astron. Inst. Czech. 38, 222.

Ceplecha, Z., Borovička, J., Elford, W.G., Revelle, D.O., Hawkes, R.L., Porubčan, V., Šimek, M., 1998. Meteor phenomena and bodies. Space Sci. Rev. 84, 327–471. http://dx.doi.org/10.1023/A:1005069928850.

Ceplecha, Z., McCrosky, R.E., 1976. Fireball end heights: A diagnostic for the structure of meteoric material. J. Geophys. Res. 81 (B35), 6257–6275. http://dx.doi.org/10.1029/JB081i035p06257.

Colas, F., Zanda, B., Bouley, S., Jeanne, S., Malgoyre, A., Birlan, M., Blanpain, C., Gattacceca, J., Jorda, L., Lecubin, J., Marmo, C., Rault, J.L., Vaubaillon, J., Vernazza, P., Yohia, C., Gardiol, D., Nedelcu, A., Poppe, B., Rowe, J., Forcier, M., Koschny, D., Trigo-Rodriguez, J.M., Lamy, H., Behrend, R., Ferrière, L., Barghini, D., Buzzoni, A., Carbognani, A., Di Carlo, M., Di Martino, M., Knapic, C., Londero, E., Pratesi, G., Rasetti, S., Riva, W., Stirpe, G.M., Valsecchi, G.B., Volpicelli, C.A., Zorba, S., Coward, D., Drolshagen, E., Drolshagen, G., Hernandez, O., Jehin, E., Jobin, M., King, A., Nitschelm, C., Ott, T., Sanchez-Lavega, A., Toni, A., Abraham, P., Affaticati, F., Albani, M., Andreis, A., Andrieu, T., Anghel, S., Antaluca, E., Antier, K., Appéré, T., Armand, A., Ascione, G., Audureau, Y., Auxepaules, G., Avoscan, T., Baba Aissa, D., Bacci, P., Bădescu, O., Baldini, R., Baldo, R., Balestrero, A., Baratoux, D., Barbotin, E., Bardy, M., Basso, S., Bautista, O., Bayle, L.D., Beck, P., Bellitto, R., Belluso, P., Benna, C., Benammi, M., Beneteau, E., Benkhaldoun, Z., Bergamini, G., Bernardi, F., Bertaina, M.E., Bessin, P., Betti, L., Bettonvil, F., Bihel, D., Birnbaum, C., Blagoi, O., Blouri, E., Boacă, I., Boată, R., Bobiet, B., Bonino, R., Boros, K., Bouchet, E., Borgeot, V., Bouchez, E., Boust, D., Boudon, V., Bouman, T., Bourget, P., Brandenburg, S., Bramond, P., Braun, E., Bussi, A., Cacault, P., Caillier, B., Calegaro, A., Camargo, J., Caminade, S., Campana, A.P.C., Campbell-Burns, P., Canal-Domingo, R., Carell, O., Carreau, S., Cascone, E., Cattaneo, C., Cauhape, M., Cavier, P., Celestin, S., Cellino, A., Champenois, M., Chennaoui Aoudjehane, H., Chevrier, S., Cholvy, P., Chomier, L., Christou, A., Cricchio, D., Coadou, P., Cocaign, J.Y., Cochard, F., Cointin, S., Colombi, E., Colque Saavedra, J.P., Corp, L., Costa, M., Costard, F., Cottier, M., Cournoyer, P., Coustal, E., Cremonese, G., Cristea, O., Cuzon, J.C., D'Agostino, G.,

Daiffallah, K., Dănescu, C., Dardon, A., Dasse, T., Davadan, C., Debs, V., Defaix, J.P., Deleflie, F., D'Elia, M., De Luca, P., De Maria, P., Deverchère, P., Devillepoix, H., Dias, A., Di Dato, A., Di Luca, R., Dominici, F.M., Drouard, A., Dumont, J.L., Dupouy, P., Duvignac, L., Egal, A., Erasmus, N., Esseiva, N., Ebel, A., Eisengarten, B., Federici, F., Feral, S., Ferrant, G., Ferreol, E., Finitzer, P., Foucault, A., Francois, P., Frîncu, M., Froger, J.L., Gaborit, F., Gagliarducci, V., Galard, J., Gardavot, A., Garmier, M., Garnung, M., Gautier, B., Gendre, B., Gerard, D., Gerardi, A., Godet, J.P., Grandchamps, A., Grouiez, B., Groult, S., Guidetti, D., Giuli, G., Hello, Y., Henry, X., Herbreteau, A., Herpin, M., Hewins, P., Hillairet, J.J., Horak, J., Hueso, R., Huet, E., Huet, S., Hyaumé, F., Interrante, G., Isselin, Y., Jeangeorges, Y., Janeux, P., Jeanneret, P., Jobse, K., Jouin, S., Jouvard, J.M., Joy, K., Julien, J.F., Kacerek, R., Kaire, M., Kempf, M., Koschny, D., Krier, C., Kwon, M.K., Lacassagne, L., Lachat, D., Lagain, A., Laisné, E., Lanchares, V., Laskar, J., Lazzarin, M., Leblanc, M., Lebreton, J.P., Lecomte, J., Le Dû, P., Lelong, F., Lera, S., Leoni, J.F., Le-Pichon, A., Le-Poupon, P., Leroy, A., Leto, G., Levansuu, J., Lewin, E., Lienard, A., Licchelli, D., Locatelli, H., Loehle, S., Loizeau, D., Luciani, L., Maignan, M., Manca, F., Mancuso, S., Mandon, E., Mangold, N., Mannucci, F., Maquet, L., Marant, D., Marchal, Y., Marin, J.L., Martin-Brisset, J.C., Martin, D., Mathieu, D., Maury, A., Mespoulet, N., Meyer, F., Meyer, J.Y., Meza, E., Moggi Cecchi, V., Moiroud, J.J., Millan, M., Montesarchio, M., Misiano, A., Molinari, E., Molau, S., Monari, S., Monflier, B., Monkos, S., Montemaggi, M., Monti, G., Moreau, R., Morin, J., Mourgues, R., Mousis, O., Nablanc, C., Nastasi, A., Niacsu, L., Notez, P., Ory, M., Pace, E., Paganelli, M.A., Pagola, A., Pajuelo, M., Palacián, J.F., Pallier, G., Paraschiv, P., Pardini, R., Pavone, M., Pavy, G., Payen, G., Pegoraro, A., Peña-Asensio, E., Perez, L., Pérez-Hoyos, S., Perlerin, V., Peyrot, A., Peth, F., Pic, V., Pietronave, S., Pilger, C., Piquel, P., Pisanu, T., Poppe, M., Portois, L., Prezeau, J.F., Pugno, N., Quantin, C., Quitté, G., Rambaux, N., Ravier, E., Repetti, U., Ribas, S., Richard, C., Richard, D., Rigoni, M., Rivet, J.P., Rizzi, N., Rochain, S., Rojas, J.F., Romeo, M., Rotaru, M., Rotger, M., Rougier, P., Rousselot, P., Rousset, J., Rousseu, D., Rubiera, O., Rudawska, R., Rudelle, J., Ruguet, J.P., Russo, P., Sales, S., Sauzereau, O., Salvati, F., Schieffer, M., Schreiner, D., Scribano, Y., Selvestrel, D., Serra, R., Shengold, L., Shuttleworth, A., Smareglia, R., Sohy, S., Soldi, M., Stanga, R., Steinhausser, A., Strafella, F., Sylla Mbaye, S., Smedley, A.R.D., Tagger, M., Tanga, P., Taricco, C., Teng, J.P., Tercu, J.O., Thizy, O., Thomas, J.P., Tombelli, M., Trangosi, R., Tregon, B., Trivero, P., Tukkers, A., Turcu, V., Umbriaco, G., Unda-Sanzana, E., Vairetti, R., Valenzuela, M., Valente, G., Varennes, G., Vauclair, S., Vergne, J., Verlinden, M., Vidal-Alaiz, M., Vieira-Martins, R., Viel, A., Vîntdevară, D.C., Vinogradoff, V., Volpini, P., Wendling, M., Wilhelm, P., Wohlgemuth, K., Yanguas, P., Zagarella, R., Zollo, A., 2020. FRIPON: a worldwide network to track incoming meteoroids. Astron. Astrophys. 644, A53. http://dx.doi.org/10.1051/0004-6361/202038649, arXiv:2012.00616.

Davis, M., Hut, P., Muller, R.A., 1984. Extinction of species by periodic comet showers. Nature 308 (5961), 715–717. http://dx.doi.org/10.1038/308715a0.

de la Fuente Marcos, R., de la Fuente Marcos, C., 2022. The closest past flyby of a known star to the solar system: HD 7977, UCAC4 237-008148 or WISE J072003.20-084651.2? Res. Not. Am. Astron. Soc. 6 (7), 152. http://dx.doi.org/10.3847/2515-5172/ac842b.

de la Fuente Marcos, C., de la Fuente Marcos, R., Aarseth, S.J., 2018. Where the solar system meets the solar neighbourhood: patterns in the distribution of radiants of observed hyperbolic minor bodies. Mon. Not. R. Astron. Soc. 476 (1), L1–L5. http://dx.doi.org/10.1093/mnrasl/sly019, arXiv:1802.00778.

de León, J., Licandro, J., de la Fuente Marcos, C., de la Fuente Marcos, R., Lara, L.M., Moreno, F., Pinilla-Alonso, N., Serra-Ricart, M., De Prá, M., Tozzi, G.P., Souza-Feliciano, A.C., Popescu, M., Scarpa, R., Font Serra, J., Geier, S., Lorenzi, V., Harutyunyan, A., Cabrera-Lavers, A., 2020. Visible and near-infrared observations of interstellar comet 2I/Borisov with the 10.4-m GTC and the 3.6-m TNG telescopes. Mon. Not. R. Astron. Soc. 495 (2), 2053–2062. http://dx.doi.org/10.1093/mnras/staa1190, arXiv:2005.00786.

Devillepoix, H.A.R., Bland, P.A., Sansom, E.K., Towner, M.C., Cupák, M., Howie, R.M., Hartig, B.A.D., Jansen-Sturgeon, T., Cox, M.A., 2019. Observation of metre-scale impactors by the desert fireball network. Mon. Not. R. Astron. Soc. 483 (4), 5166–5178. http://dx.doi.org/10.1093/mnras/sty3442, arXiv:1808.09195.

Dmitriev, V., Lupovka, V., Gritsevich, M., 2015. Orbit determination based on meteor observations using numerical integration of equations of motion. Planet. Space Sci. 117, 223–235. http://dx.doi.org/10.1016/j.pss.2015.06.015.

Dones, L., Weissman, P.R., Levison, H.F., Duncan, M.J., 2004. Oort cloud formation and dynamics. In: Festou, M.C., Keller, H.U., Weaver, H.A. (Eds.), Comets II. The University of Arizona Press, p. 153.

Drolshagen, E., Ott, T., Koschny, D., Drolshagen, G., Vaubaillon, J., Colas, F., Zanda, B., Bouley, S., Jeanne, S., Malgoyre, A., Birlan, M., Vernazza, P., Gardiol, D., Nedelcu, D.A., Rowe, J., Forcier, M., Trigo-Rodriguez, J.M., Peña-Asensio, E., Lamy, H., Ferrière, L., Barghini, D., Carbognani, A., Di Martino, M., Rasetti, S., Valsecchi, G.B., Volpicelli, C.A., Di Carlo, M., Knapic, C., Pratesi, G., Riva, W., Stirpe, G.M., Zorba, S., Hernandez, O., Grandchamps, A., Jehin, E., Jobin, M., King, A., Sanchez-Lavega, A., Toni, A., Rimola, A., Poppe, B., 2021a. Luminous efficiency based on FRIPON meteors and limitations of ablation models. Astron. Astrophys. 650, A159. http://dx.doi.org/10.1051/0004-6361/202040204.

Drolshagen, E., Ott, T., Koschny, D., Drolshagen, G., Vaubaillon, J., Colas, F., Zanda, B., Bouley, S., Jeanne, S., Malgoyre, A., Birlan, M., Vernazza, P., Gardiol, D., Nedelcu, D.A., Rowe, J., Forcier, M., Trigo-Rodriguez, J.M., Peña-Asensio, E., Lamy, H., Ferrière, L., Barghini, D., Carbognani, A., Di Martino, M., Rasetti, S., Valsecchi, G.B., Volpicelli, C.A., Di Carlo, M., Knapic, C., Pratesi, G., Riva, W., Stirpe, G.M., Zorba, S., Hernandez, O., Grandchamps, A., Jehin, E., Jobin, M., King, A., Sanchez-Lavega, A., Toni, A., Rimola, A., Poppe, B., 2021b. Luminous efficiency of meteors derived from ablation model after assessment of its range of validity. Astron. Astrophys. 652, A84. http://dx.doi.org/10.1051/0004-6361/202140917.

Drummond, J.D., 1981. A test of comet and meteor shower associations. Icarus 45 (3), 545–553. http://dx.doi.org/10.1016/0019-1035(81)90020-8.

Dupuy, T.J., Liu, M.C., Best, W.M.J., Mann, A.W., Tucker, M.A., Zhang, Z., Baraffe, I., Chabrier, G., Forveille, T., Metchev, S.A., Tremblin, P., Do, A., Payne, A.V., Shappee, B.J., Bond, C.Z., Cetre, S., Chun, M., Delorme, J.-R., Jovanovic, N., Lilley, S., Mawet, D., Ragland, S., Wetherell, E., Wizinowich, P., 2019. WISE J072003.20-084651.2b is a massive t dwarf. Astron. J. 158 (5), 174. http://dx.doi.org/10.3847/1538-3881/ab3cd1, arXiv:1908.06994.

Dybczyński, P.A., Królikowska, M., 2022. The influence of individual stars on the long-term dynamics of comets C/2014 UN₂₇₁ and C/2017 K2. Astron. Astrophys. 660, A100. http://dx.doi.org/10.1051/0004-6361/202143018, arXiv:2112.15353.

Egal, A., Gural, P.S., Vaubaillon, J., Colas, F., Thuillot, W., 2017. The challenge associated with the robust computation of meteor velocities from video and photographic records. Icarus 294, 43–57. http://dx.doi.org/10.1016/j.icarus.2017.04.024.

Engelhardt, T., Jedicke, R., Vereš, P., Fitzsimmons, A., Denneau, L., Beshore, E., Meinke, B., 2017. An observational upper limit on the interstellar number density of asteroids and comets. Astron. J. 153 (3), 133. http://dx.doi.org/10.3847/1538-3881/aa5c8a, arXiv:1702.02237.

Fouchard, M., Rickman, H., Froeschlé, C., Valsecchi, G.B., 2011. The last revolution of new comets: the role of stars and their detectability. Astron. Astrophys. 535, A86. http://dx.doi.org/10.1051/0004-6361/201116514.

Froncisz, M., Brown, P., Weryk, R.J., 2020. Possible interstellar meteoroids detected by the Canadian meteor orbit radar. Planet. Space Sci. 190, 104980. http://dx.doi.org/10.1016/j.pss.2020.104980, arXiv:2005.10896.

Galligan, D.P., 2001. Performance of the D-criteria in recovery of meteoroid stream orbits in a radar data set. Mon. Not. R. Astron. Soc. 327 (2), 623–628. http://dx.doi.org/10.1046/j.1365-8711.2001.04858.x.

Gritsevich, M.I., 2007. Approximation of the observed motion of bolides by the analytical solution of the equations of meteor physics. Solar Syst. Res. 41 (6), 509–514. http://dx.doi.org/10.1134/S003809460706007X.

Gritsevich, M.I., 2008. The pribram, lost city, innisfree, and neuschwanstein falls: An analysis of the atmospheric trajectories. Solar Syst. Res. 42 (5), 372–390. http://dx.doi.org/10.1134/S003809460805002X.

Gritsevich, M.I., 2009. Determination of parameters of meteor bodies based on flight observational data. Adv. Space Res. 44 (3), 323–334. http://dx.doi.org/10.1016/j.asr.2009.03.030.

Gritsevich, M., Koschny, D., 2011. Constraining the luminous efficiency of meteors. Icarus 212 (2), 877–884. http://dx.doi.org/10.1016/j.icarus.2011.01.033.

Gritsevich, M.I., Lukashenko, V., Turchak, L., 2016. Approximating the solution of meteor physics equations through the use of elementary functions. Math. Models Comput. Simul. 8, 1–6.

Gritsevich, M., Lyytinen, E., Moilanen, J., Kohout, T., Dmitriev, V., Lupovka, V., Midtskogen, I., Kruglikov, N., Ischenko, A., Yakovlev, G., Grokhovsky, V., Haloda, J., Halodova, P., Peltoniemi, J., Aikkila, A., Taavitsainen, A., Lauanne, J., Pekkola, M., Kokko, P., Lahtinen, P., Larionov, M., 2014. First meteorite recovery based on observations by the finnish fireball network. In: Rault, J.L., Roggemans, P. (Eds.), Proceedings of the International Meteor Conference, Giron, France, 18-21 September 2014. pp. 162–169.

Gritsevich, M.I., Popelenskaya, N.V., 2008. Meteor and fireball trajectories for high values of the mass loss parameter. Physics (Doklady) 53 (2), 88–92. http://dx.doi.org/10.1134/S1028335808020092.

Gritsevich, M.I., Stulov, V.P., 2006. Extra-atmospheric masses of the Canadian network bolides. Solar Syst. Res. 40 (6), 477–484. http://dx.doi.org/10.1134/S0038094606060050.

Gritsevich, M.I., Stulov, V.P., Turchak, L.I., 2012. Consequences of collisions of natural cosmic bodies with the earth's atmosphere and surface. Cosmic Res. 50 (1), 56–64. http://dx.doi.org/10.1134/S0010952512010017.

Guzik, P., Drahus, M., Rusek, K., Waniak, W., Cannizzaro, G., Pastor-Marazuela, I., 2020. Initial characterization of interstellar comet 2I/borisov. Nat. Astron. 4, 53–57. http://dx.doi.org/10.1038/s41550-019-0931-8, arXiv:1909.05851.

Hajduková, M., 2008. Meteors in the IAU meteor data center on hyperbolic orbits. Earth Moon Planets 102 (1–4), 67–71. http://dx.doi.org/10.1007/s11038-007-9171-5.

Hajduková, M., Kornoš, L., Tóth, J., 2014. Frequency of hyperbolic and interstellar meteoroids. Meteorit. Planet. Sci. 49 (1), 63–68. http://dx.doi.org/10.1111/maps.12119.

Hajduková, Mária, J., Sterken, V., Wiegert, P., 2019. Interstellar meteoroids. In: Ryabova, G.O., Asher, D.J., Campbell-Brown, M.J. (Eds.), Meteoroids: Sources of Meteors on Earth and beyond. Cambridge University Press, p. 235.

Hajdukova, M., Sterken, V., Wiegert, P., Kornoš, L., 2020. The challenge of identifying interstellar meteors. Planet. Space Sci. 192, 105060. http://dx.doi.org/10.1016/j.pss.2020.105060.

Hanse, J., Jílková, L., Portegies Zwart, S.F., Pelupessy, F.I., 2018. Capture of exocomets and the erosion of the oort cloud due to stellar encounters in the galaxy. Mon. Not. R. Astron. Soc. 473 (4), 5432–5445. http://dx.doi.org/10.1093/mnras/stx2721, arXiv:1710.05866.

Higuchi, A., Kokubo, E., 2020. Hyperbolic orbits in the solar system: Interstellar origin or perturbed oort cloud comets? Mon. Not. R. Astron. Soc. 492 (1), 268–275. http://dx.doi.org/10.1093/mnras/stz3153, arXiv:1911.04524.

Hildebrand, A.R., Hanton, L.T.J., Ciceri, F., Nowell, R., Lyytinen, E., Silber, E.A., Brown, P.G., Gi, N., Jenniskens, P.M.M., Albers, J., Hladiuk, D., 2018. Characteristics of a well recorded, bright, meteorite-dropping fireball, british columbia, Canada, september 4, 2017. In: 49th Annual Lunar and Planetary Science Conference. In: Lunar and Planetary Science Conference, p. 3006.

Hughes, D.W., 1982. The history of meteors and meteor showers. Vistas Astron. 26 (4), 325–345. http://dx.doi.org/10.1016/0083-6656(82)90010-1.

Jenniskens, P., Gabadirwe, M., Yin, Q.-Z., Proyer, A., Moses, O., Kohout, T., Franchi, F., Gibson, R.L., Kowalski, R., Christensen, E.J., Gibbs, A.R., Heinze, A., Denneau, L., Farnocchia, D., Chodas, P.W., Gray, W., Micheli, M., Moskovitz, N., Onken, C.A., Wolf, C., Devillepoix, H.A.R., Ye, Q., Robertson, D.K., Brown, P., Lyytinen, E., Moilanen, J., Albers, J., Cooper, T., Assink, J., Evers, L., Lahtinen, P., Seitshiro, L., Laubenstein, M., Wantlo, N., Moleje, P., Maritinkole, J., Suhonen, H., Zolensky, M.E., Ashwal, L., Hiroi, T., Sears, D.W., Sehlke, A., Maturilli, A., Sanborn, M.E., Huyskens, M.H., Dey, S., Ziegler, K., Busemann, H., Riebe, M.E.I., Meier, M.M.M., Welten, K.C., Caffee, M.W., Zhou, Q., Li, Q.-L., Li, X.-H., Liu, Y., Tang, G.-Q., McLain, H.L., Dworkin, J.P., Glavin, D.P., Schmitt-Kopplin, P., Sabbah, H., Joblin, C., Granvik, M., Mosarwa, B., Botepe, K., 2021. The impact and recovery of asteroid 2018 LA. Meteorit. Planet. Sci. 56 (4), 844–893. http://dx.doi.org/10.1111/maps.13653, URL: https://onlinelibrary.wiley.com/doi/abs/10.1111/maps.13653. arXiv:https://onlinelibrary.wiley.com/doi/pdf/10.1111/maps.13653.

Jenniskens, P., Shaddad, M.H., Numan, D., Elsir, S., Kudoda, A.M., Zolensky, M.E., Le, L., Robinson, G.A., Friedrich, J.M., Rumble, D., Steele, A., Chesley, S.R., Fitzsimmons, A., Duddy, S., Hsieh, H.H., Ramsay, G., Brown, P.G., Edwards, W.N., Tagliaferri, E., Boslough, M.B., Spalding, R.E., Dantowitz, R., Kozubal, M., Pravec, P., Borovicka, J., Charvat, Z., Vaubaillon, J., Kuiper, J., Albers, J., Bishop, J.L., Mancinelli, R.L., Sandford, S.A., Milam, S.N., Nuevo, M., Worden, S.P., 2009. The impact and recovery of asteroid 2008 TC$_3$. Nature 458 (7237), 485–488. http://dx.doi.org/10.1038/nature07920.

Jewitt, D., Luu, J., Rajagopal, J., Kotulla, R., Ridgway, S., Liu, W., Augusteijn, T., 2017. Interstellar Interloper 1I/2017 U1: Observations from the NOT and WIYN Telescopes. The Astrophysical Journal Letters 850 (2), L36. http://dx.doi.org/10.3847/2041-8213/aa9b2f.

Jewitt, D., Seligman, D.Z., 2023. The interstellar interlopers. Annu. Rev. Astron. Astrophys. 61, 197–236. http://dx.doi.org/10.1146/annurev-astro-071221-054221, arXiv:2209.08182.

JPL Horizons, 2023. Horizons system, JPL website. https://ssd.jpl.nasa.gov/horizons/. Accessed: 2023-10-03.

Kartashova, A., Golubaev, A., Mozgova, A., Chuvashov, I., Bolgova, G., Glazachev, D., Efremov, V., 2020. Investigation of the ozerki meteoroid parameters. Planet. Space Sci. 193, 105034. http://dx.doi.org/10.1016/j.pss.2020.105034.

Kiefer, F., Lecavelier des Etangs, A., Boissier, J., Vidal-Madjar, A., Beust, H., Lagrange, A.M., Hébrard, G., Ferlet, R., 2014. Two families of exocomets in the β pictoris system. Nature 514 (7523), 462–464. http://dx.doi.org/10.1038/nature13849.

Królikowska, M., Dybczyński, P.A., 2017. Oort spike comets with large perihelion distances. Mon. Not. R. Astron. Soc. 472 (4), 4634–4658. http://dx.doi.org/10.1093/mnras/stx2157, arXiv:1708.09248.

Kulakov, A.L., Stulov, V.P., 1992. Determination of meteor body parameters from observational data. Astron. Vestn. 26 (5), 67–75.

Kyrylenko, I., Golubov, O., Slyusarev, I., Visuri, J., Gritsevich, M., Krugly, Y.N., Belskaya, I., Shevchenko, V.G., 2023. The first instrumentally documented fall of an iron meteorite: Orbit and possible origin. Astrophys. J. 953 (1), 20. http://dx.doi.org/10.3847/1538-4357/acdc21.

Lyytinen, E., Gritsevich, M., 2016. Implications of the atmospheric density profile in the processing of fireball observations. Planet. Space Sci. 120, 35–42. http://dx.doi.org/10.1016/j.pss.2015.10.012.

Maksimova, A.A., Petrova, E.V., Chukin, A.V., Karabanalov, M.S., Felner, I., Gritsevich, M., Oshtrakh, M.I., 2020. Characterization of the matrix and fusion crust of the recent meteorite fall ozerki L6. Meteorit. Planet. Sci. 55 (1), 231–244. http://dx.doi.org/10.1111/maps.13423.

Mamajek, E.E., Barenfeld, S.A., Ivanov, V.D., Kniazev, A.Y., Väisänen, P., Beletsky, Y., Boffin, H.M.J., 2015. The closest known flyby of a star to the solar system. Astrophys. J. Lett. 800 (1), L17. http://dx.doi.org/10.1088/2041-8205/800/1/L17, arXiv:1502.04655.

Marois, C., Zuckerman, B., Konopacky, Q.M., Macintosh, B., Barman, T., 2010. Images of a fourth planet orbiting HR 8799. Nature 468 (7327), 1080–1083. http://dx.doi.org/10.1038/nature09684, arXiv:1011.4918.

Meech, K.J., Weryk, R., Micheli, M., Kleyna, J.T., Hainaut, O.R., Jedicke, R., Wainscoat, R.J., Chambers, K.C., Keane, J.V., Petric, A., Denneau, L., Magnier, E., Berger, T., Huber, M.E., Flewelling, H., Waters, C., Schunova-Lilly, E., Chastel, S., 2017. A brief visit from a red and extremely elongated interstellar asteroid. Nature 552 (7685), 378–381. http://dx.doi.org/10.1038/nature25020.

Meisel, D.D., Janches, D., Mathews, J.D., 2002a. Extrasolar micrometeors radiating from the vicinity of the local interstellar bubble. Astrophys. J. 567 (1), 323–341. http://dx.doi.org/10.1086/322317.

Meisel, D.D., Janches, D., Mathews, J.D., 2002b. The size distribution of arecibo interstellar particles and its implications. Astrophys. J. 579 (2), 895–904. http://dx.doi.org/10.1086/342919.

Milley, E.P., 2010. Physical Properties of Fireball-Producing Earth-Impacting Meteoroids and Orbit Determination through Shadow Calibration of the Buzzard Coulee Meteorite Fall (Master's thesis). University of Calgary, Canada.

Moilanen, J., Gritsevich, M., Lyytinen, E., 2021. Determination of strewn fields for meteorite falls. Mon. Not. R. Astron. Soc. 503 (3), 3337–3350. http://dx.doi.org/10.1093/mnras/stab586.

Moreno-Ibáñez, M., Gritsevich, M., Trigo-Rodríguez, J.M., 2015. New methodology to determine the terminal height of a fireball. Icarus 250, 544–552. http://dx.doi.org/10.1016/j.icarus.2014.12.027, arXiv:1502.01898.

Moreno-Ibáñez, M., Gritsevich, M., Trigo-Rodríguez, J.M., 2017. Measuring the terminal heights of bolides to understand the atmospheric flight of large asteroidal fragments. In: Trigo-Rodríguez, J.M., Gritsevich, M., Palme, H. (Eds.), Assessment and Mitigation of Asteroid Impact Hazards: Proceedings of the 2015 Barcelona Asteroid Day. In: Astrophysics and Space Science Proceedings, vol. 46, p. 129. http://dx.doi.org/10.1007/978-3-319-46179-3_7.

Moreno-Ibáñez, M., Gritsevich, M., Trigo-Rodríguez, J.M., Silber, E.A., 2020. Physically based alternative to the PE criterion for meteoroids. Mon. Not. R. Astron. Soc. 494 (1), 316–324. http://dx.doi.org/10.1093/mnras/staa646, arXiv:2002.12842.

Musci, R., Weryk, R.J., Brown, P., Campbell-Brown, M.D., Wiegert, P.A., 2012. An optical survey for millimeter-sized interstellar meteoroids. Astrophys. J. 745 (2), 161. http://dx.doi.org/10.1088/0004-637X/745/2/161, arXiv:1110.5882.

Oort, J.H., 1950. The structure of the cloud of comets surrounding the solar system and a hypothesis concerning its origin. Bull. Astron. Inst. Netherlands 11, 91–110.

Opik, E.J., 1950. Interstellar meteors and related problems. Ir. Astron. J. 1, 80.

Peña-Asensio, E., Trigo-Rodríguez, J.M., Gritsevich, M., Rimola, A., 2021a. Accurate 3D fireball trajectory and orbit calculation using the 3D-FIRETOC automatic python code. Mon. Not. R. Astron. Soc. 504 (4), 4829–4840. http://dx.doi.org/10.1093/mnras/stab999, arXiv:2103.13758.

Peña-Asensio, E., Trigo-Rodríguez, J.M., Langbroek, M., Rimola, A., Robles, A.J., 2021b. Using fireball networks to track more frequent reentries: Falcon 9 upper-stage orbit determination from video recordings. Astrodynamics 5 (4), 347–358. http://dx.doi.org/10.1007/s42064-021-0112-2, arXiv:2109.01004.

Peña-Asensio, E., Trigo-Rodríguez, J.M., Rimola, A., 2022. Orbital characterization of superbolides observed from space: Dynamical association with near-earth objects, meteoroid streams, and identification of hyperbolic meteoroids. Astron. J. 164 (3), 76. http://dx.doi.org/10.3847/1538-3881/ac75d2, arXiv:2206.03115.

Peña-Asensio, E., Trigo-Rodríguez, J.M., Rimola, A., Corretgé-Gilart, M., Koschny, D., 2023. Identifying meteorite droppers among the population of bright 'sporadic' bolides imaged by the spanish meteor network during the spring of 2022. Mon. Not. R. Astron. Soc. 520 (4), 5173–5182. http://dx.doi.org/10.1093/mnras/stad102, arXiv:https://academic.oup.com/mnras/article-pdf/520/4/5173/49329818/stad102.pdf.

Rein, H., Spiegel, D.S., 2015. IAS15: a fast, adaptive, high-order integrator for gravitational dynamics, accurate to machine precision over a billion orbits. Mon. Not. R. Astron. Soc. 446 (2), 1424–1437. http://dx.doi.org/10.1093/mnras/stu2164, arXiv:1409.4779.

Revelle, D.O., Ceplecha, Z., 2001. Bolide physical theory with application to PN and EN fireballs. In: Warmbein, B. (Ed.), Meteoroids 2001 Conference. In: ESA Special Publication, vol. 495, pp. 507–512.

Rickman, H., Fouchard, M., Valsecchi, G.B., Froeschlé, C., 2005. Algorithms for stellar perturbation computations on oort cloud comets. Earth Moon Planets 97 (3–4), 411–434. http://dx.doi.org/10.1007/s11038-006-9113-7.

Sansom, E.K., Gritsevich, M., Devillepoix, H.A.R., Jansen-Sturgeon, T., Shober, P., Bland, P.A., Towner, M.C., Cupák, M., Howie, R.M., Hartig, B.A.D., 2019a. Determining fireball fates using the α-β criterion. Astrophys. J. 885 (2), 115. http://dx.doi.org/10.3847/1538-4357/ab4516, arXiv:1909.11494.

Sansom, E.K., Jansen-Sturgeon, T., Rutten, M.G., Devillepoix, H.A.R., Bland, P.A., Howie, R.M., Cox, M.A., Towner, M.C., Cupák, M., Hartig, B.A.D., 2019b. 3D meteoroid trajectories. Icarus 321, 388–406. http://dx.doi.org/10.1016/j.icarus.2018.09.026, arXiv:1802.02697.

Scheirich, P., Durech, J., Pravec, P., Kozubal, M., Dantowitz, R., Kaasalainen, M., Betzler, A.S., Beltrame, P., Muler, G., Birthwhistle, P., Kugel, F., 2010. The shape and rotation of asteroid 2008 TC$_3$. Meteorit. Planet. Sci. 45 (1804), 1804–1811. http://dx.doi.org/10.1111/j.1945-5100.2010.01146.x.

Scholz, R.D., 2014. Neighbours hiding in the galactic plane, a new M/L dwarf candidate for the 8 pc sample. Astron. Astrophys. 561, A113. http://dx.doi.org/10.1051/0004-6361/201323015, arXiv:1311.2716.

Seligman, D.Z., Moro-Martín, A., 2023. Interstellar objects. Contemp. Phys. 1–33. http://dx.doi.org/10.1080/00107514.2023.2203976.

Shannon, A., Jackson, A.P., Wyatt, M.C., 2019. Oort cloud asteroids: collisional evolution, the nice model, and the grand tack. Mon. Not. R. Astron. Soc. 485 (4), 5511–5518. http://dx.doi.org/10.1093/mnras/stz776, arXiv:1903.03199.

Shober, P.M., Jansen-Sturgeon, T., Sansom, E.K., Devillepoix, H.A.R., Towner, M.C., Bland, P.A., Cupák, M., Howie, R.M., Hartig, B.A.D., 2020. Where did they come from, where did they go: Grazing fireballs. Astron. J. 159 (5), 191. http://dx.doi.org/10.3847/1538-3881/ab8002, arXiv:1912.01895.

Silber, E.A., Boslough, M., Hocking, W.K., Gritsevich, M., Whitaker, R.W., 2018. Physics of meteor generated shock waves in the earth's atmosphere - a review. Adv. Space Res. 62 (3), 489–532. http://dx.doi.org/10.1016/j.asr.2018.05.010, arXiv:1805.07842.

Siraj, A., Loeb, A., 2022a. A meteor of apparent interstellar origin in the CNEOS fireball catalog. Astrophys. J. 939 (1), 53. http://dx.doi.org/10.3847/1538-4357/ac8eac.

Siraj, A., Loeb, A., 2022b. Interstellar meteors are outliers in material strength. Astrophys. J. Lett. 941 (2), L28. http://dx.doi.org/10.3847/2041-8213/aca8a0, arXiv:2209.09905.

Socas-Navarro, H., 2019. Can a negative-mass cosmology explain dark matter and dark energy? Astron. Astrophys. 626, A5. http://dx.doi.org/10.1051/0004-6361/201935317, arXiv:1902.08287.

Socas-Navarro, H., 2023. A candidate location for planet nine from an interstellar meteoroid: The messenger hypothesis. Astrophys. J. 945 (1), 22. http://dx.doi.org/10.3847/1538-4357/acb817, arXiv:2205.07675.

Stern, A., 1987. Extra-solar oort cloud encounters and planetary impact rates. Icarus 69 (1), 185–188. http://dx.doi.org/10.1016/0019-1035(87)90013-3.

Stulov, V.P., 1997. Interactions of space bodies with atmospheres of planets. Appl. Mech. Rev. 50, 671. http://dx.doi.org/10.1115/1.3101678.

Stulov, V.P., 1998. Gasdynamical model of the tunguska fall. Planet. Space Sci. 46 (2), 253–260. http://dx.doi.org/10.1016/S0032-0633(97)00082-2.

Stulov, V.P., 2004. Asymptotic theory of the motion of celestial bodies in the atmosphere. Planet. Space Sci. 52 (5–6), 459–463. http://dx.doi.org/10.1016/j.pss.2003.07.005.

Subasinghe, D., Campbell-Brown, M., Stokan, E., 2017. Luminous efficiency estimates of meteors -I. Uncertainty analysis. Planet. Space Sci. 143, 71–77. http://dx.doi.org/10.1016/j.pss.2016.12.009, arXiv:1704.08656.

Tagliaferri, E., Spalding, R., Jacobs, C., Worden, S.P., Erlich, A., 1994. Detection of meteoroid impacts by optical sensors in earth orbit. In: Hazards Due to Comets and Asteroids. p. 199.

Tamayo, D., Rein, H., Shi, P., Hernandez, D.M., 2020. REBOUNDx: a library for adding conservative and dissipative forces to otherwise symplectic N-body integrations. Mon. Not. R. Astron. Soc. 491 (2), 2885–2901. http://dx.doi.org/10.1093/mnras/stz2870, arXiv:1908.05634.

Trigo-Rodríguez, J.M., 2019. The flux of meteoroids over time: meteor emission spectroscopy and the delivery of volatiles and chondritic materials to earth. In: Hypersonic Meteoroid Entry Physics. IOP Publishing, p. 4. http://dx.doi.org/10.1088/2053-2563/aae894ch4.

Trigo-Rodríguez, J.M., Blum, J., 2022. Learning about comets from the study of mass distributions and fluxes of meteoroid streams. Mon. Not. R. Astron. Soc. 512 (2), 2277–2289. http://dx.doi.org/10.1093/mnras/stab2827, arXiv:2109.14428.

Trigo-Rodríguez, J.M., Llorca, J., 2006. The strength of cometary meteoroids: clues to the structure and evolution of comets. Mon. Not. R. Astron. Soc. 372 (2), 655–660. http://dx.doi.org/10.1111/j.1365-2966.2006.10843.x.

Trigo-Rodríguez, J.M., Llorca, J., Castro-Tirado, A.J., Ortiz, J.L., Docobo, J.A., Fabregat, J., 2006. The spanish fireball network. Astron. Geophys. 47 (2), 6.26–6.28. http://dx.doi.org/10.1111/j.1468-4004.2006.47626.x.

Trigo-Rodríguez, J.M., Lyytinen, E., Gritsevich, M., Moreno-Ibáñez, M., Bottke, W.F., Williams, I., Lupovka, V., Dmitriev, V., Kohout, T., Grokhovsky, V., 2015. Orbit and dynamic origin of the recently recovered annama's H5 chondrite. Mon. Not. R. Astron. Soc. 449 (2), 2119–2127. http://dx.doi.org/10.1093/mnras/stv378, arXiv:1507.04342.

Turchak, L.I., Gritsevich, M.I., 2014. Meteoroids interaction with the earth atmosphere. J. Theoret. Appl. Mech. 44 (4), 15–28. http://dx.doi.org/10.2478/jtam-2014-0020.

Unsalan, O., Jenniskens, P., Yin, Q.-Z., Kaygisiz, E., Albers, J., Clark, D.L., Granvik, M., Demirkol, I., Erdogan, I.Y., Bengu, A.S., Özel, M.E., Terzioglu, Z., Gi, N., Brown, P., Yalcinkaya, E., Temel, T., Prabhu, D.K., Robertson, D.K., Boslough, M., Ostrowski, D.R., Kimberley, J., Er, S., Rowland, D.J., Bryson, K.L., Altunayar-Unsalan, C., Ranguelov, B., Karamanov, A., Tatchev, D., Kocahan, Ö., Oshtrakh, M.I., Maksimova, A.A., Karabanalov, M.S., Verosub, K.L., Levin, E., Uysal, I., Hoffmann, V., Hiroi, T., Reddy, V., Ildiz, G.O., Bolukbasi, O., Zolensky, M.E., Hochleitner, R., Kaliwoda, M., Öngen, S., Fausto, R., Nogueira, B.A., Chukin, A.V., Karashanova, D., Semionkin, V.A., YeşIltaş, M., Glotch, T., Yilmaz, A., Friedrich, J.M., Sanborn, M.E., Huyskens, M., Ziegler, K., Williams, C.D., SchöN-bäChler, M., Bauer, K., Meier, M.M.M., Maden, C., Busemann, H., Welten, K.C., Caffee, M.W., Laubenstein, M., Zhou, Q., Li, Q.-L., Li, X.-H., Liu, Y., Tang, G.-Q., Sears, D.W.G., McLain, H.L., Dworkin, J.P., Elsila, J.E., Glavin, D.P., Schmitt-Kopplin, P., Ruf, A., Le Corre, L., Schmedemann, N., Sariçiček Meteorite Consortiu, 2019. The sariçiçek howardite fall in Turkey: Source crater of HED meteorites on vesta and impact risk of vestoids. Meteorit. Planet. Sci. 54 (5), 953–1008. http://dx.doi.org/10.1111/maps.13258, arXiv:2102.03733.

Vaubaillon, J., 2022. Hyperbolic meteors: is CNEOS 2014-01-08 interstellar? WGN J. Int. Meteorl. Organ. 50 (5), 140–143. http://dx.doi.org/10.48550/arXiv.2211.02305, arXiv:2211.02305.

Vida, D., Brown, P.G., Campbell-Brown, M., 2018. Modelling the measurement accuracy of pre-atmosphere velocities of meteoroids. Mon. Not. R. Astron. Soc. 479 (4), 4307–4319. http://dx.doi.org/10.1093/mnras/sty1841, arXiv:1807.03213.

Vida, D., Brown, P.G., Devillepoix, H.A.R., Wiegert, P., Moser, D.E., Matlovič, P., Herd, C.D.K., Hill, P.J.A., Sansom, E.K., Towner, M.C., Tóth, J., Cooke, W.J., Hladiuk, D.W., 2023. Direct measurement of decimetre-sized rocky material in the oort cloud. Nat. Astron. 7, 318–329. http://dx.doi.org/10.1038/s41550-022-01844-3, arXiv:2212.06812.

Vida, D., Šegon, D., Šegon, M., Atanackov, J., Ambrožič, B., McFadden, L., Ferrière, L., Kac, J., Kladnik, G., Živčić, M., Merlak, A., Skokić, I., Pavletić, L., Vinčić, G., Ćiković, I., Perkó, Z., Ilari, M., Malarić, M., Macuka, I., 2021. Novo mesto meteorite fall - trajectory, orbit, and fragmentation analysis from optical observations. In: European Planetary Science Congress. pp. EPSC2021–EPSC2139. http://dx.doi.org/10.5194/epsc2021-139.

Visuri, J.J., Gritsevich, M.I., 2021. Introducing the FireOwl — data processing software of the finnish fireball network. In: 84th Annual Meeting of the Meteoritical Society. In: LPI Contributions, vol. 84, p. 6093.

Visuri, J., Lyytinen, E., Sievinen, J., Gritsevich, M., 2020. Correcting the atmospheric refraction of fireball observations at low elevation angles and significance of the correction. In: European Planetary Science Congress. pp. EPSC2020–EPSC2526. http://dx.doi.org/10.5194/epsc2020-526.

Štohl, J., 1970. On the problem of hyperbolic meteors. Bull. Astron. Inst. Czech. 21, 10.

Weryk, R.J., Brown, P., 2004. A search for interstellar meteoroids using the Canadian meteor orbit radar (CMOR). Earth Moon Planets 95 (1–4), 221–227. http://dx.doi.org/10.1007/s11038-005-9034-x.

Weryk, R.J., Brown, P.G., 2013. Simultaneous radar and video meteors—II: Photometry and ionisation. Planet. Space Sci. 81, 32–47. http://dx.doi.org/10.1016/j.pss.2013.03.012.

Whipple, F.L., Jacchia, L.G., 1957. Reduction methods for photographic meteor trails. Smithson. Contrib. Astrophys. 1, 183–206.

Wiegert, P.A., 2014. Hyperbolic meteors: Interstellar or generated locally via the gravitational slingshot effect? Icarus 242, 112–121. http://dx.doi.org/10.1016/j.icarus.2014.06.031, arXiv:1404.2159.

Wilson, T., 2018. Evaluating the the Effectiveness of Current Atmospheric Refraction Models in Predicting Sunrise and Sunset Times (Ph.D. thesis). Michigan Technological University.

Zuluaga, J.I., Cuartas-Restrepo, P.A., Ospina, J., Sucerquia, M., 2019. Can we predict the impact conditions of metre-sized meteoroids? Mon. Not. R. Astron. Soc. 486 (1), L69–L73. http://dx.doi.org/10.1093/mnrasl/slz060, arXiv:1902.03980.